Univerzita Karlova v Praze

Přírodovědecká fakulta

Studijní program: **Chemie**

Studijní obor: **Modelování chemických vlastností nano- a biostruktur**

Bc. Miroslav Položij

Teoretické studium mechanismů chemických reakcí probíhajících v mikroporézních materiálech

Theoretical Investigation of Mechanisms of Chemical Reactions Taking Place in Microporous Materials

Diplomová práce

Školitel: Doc. RNDr. Petr Nachtigall PhD.

Praha, 2013

Prohlášení:

Prohlašuji, že jsem závěrečnou práci zpracoval samostatně a že jsem uvedl všechny použité informační zdroje a literaturu. Tato práce ani její podstatná část nebyla předložena k získání jiného nebo stejného akademického titulu.

V Praze, 17.05.2013

Podpis

I would like to thank my advisor prof. Peter Nachtigall for his patience, support and guidance, as well as my colleagues for their good advices. I would also like to thank my family and friends for their support during my studies.

Abstract:

Mechanisms of three reactions catalyzed by microporous materials were investigated computationally; the reactions investigated include Friedländer and Knoevenagel reactions catalyzed by Cu_3BTC_2 metal organic framework (MOF) and an intramolecular cyclisation of unsaturated alcohols catalyzed by zeolite H-ZSM-5. It was found that the reaction mechanisms of all three reactions are controlled by a high concentration of active sites in materials. Reaction intermediates interact with more than one active site simultaneously. This novel concept of "multiple-site" interactions is described. The concerted effect of two catalytic sites leads to a decrease of activation barriers on reaction paths of Friedländer and Knoevenagel reactions. On the contrary, a simultaneous interaction of reactants with two active sites has a negative effect on reaction rate in case of alcohol cyclization catalyzed by H-ZSM-5; it was found that the interaction with dual sites results in the increase of activation barriers and diffusion limitations. In case of Knoevenagel reaction catalyzed by CuBTC, the adsorption of reaction precursor to the reaction site allows the creation of a dynamic defect in the MOF framework that subsequently catalyses the reaction. Both, the multiple sites effect and the dynamical defect formation effect are novel concepts that offer explanations of some properties of microporous materials.

Keywords: metal-organic frameworks, DFT, Friedländer reaction, Knoevenagel reaction, heterocycles, multiple-site interaction

Abstrakt:

Pomocí výpočetních metod byly zkoumány mechanismy tří chemických reakcí: Friedländerovy a Knoevenagelovy reakce katalyzované organokovovým materiálem (tzv. „metal-organic framework") Cu_3BTC_2 a intramolekulární cyklizace nesaturovaných alkoholů katalyzovaná zeolitem H-ZSM-5. Bylo zjištěno, že reakční mechanismus všech tří reakcí je ovlivňován vysokou koncentrací aktivních míst v použitých katalyzátorech. Vysoká koncentrace adsorpčních míst dovoluje interakci reakčních intermediátů s více aktivními místy zároveň. V případě Friedländerovy a Knoevenagelovy reakce dochází ke snížení aktivačních bariér v důsledku interakce reakčních intermediátů se dvěma katalyticky aktivními místy současně. Opačný efekt byl nalezen pro cyklizaci alkoholů v zeolitu, pro kterou bylo zjištěno, že současná interakce s dvěma aktivními místy zvedne aktivační bariéru reakce a zároveň omezí difúzi uvnitř zeolitu. Studie reakčního mechanismu Knoevenagelovy reakce odhalila (doposud nepopsanou) dynamickou tvorbu defektů v mříži organokovového materiálu. Tento defekt následně katalyzuje Knoevenagelovu reakci. Oba nově popsané efekty nabízí interpretaci dalších vlastností mikroporézních katalyzátorů s vysokou koncentrací aktivních míst.

Klíčová slova: metal-organic frameworks, DFT, Friedländerova reakce, Knoevenagelova reakce, heterocykly, vícenásobná interakce

Contents

The list of abbreviations

B3LYP	hybrid exchange-correlation functional using Becke's functional B and Lee-Yang-Par functional LYP
BTC	Benzene-1,3,5-tricarboxylate
cus	coordinatively unsaturated site
DFT	Density Functional Theory
FTIR	Fourier Transform Infrared Spectroscopy
GGA	Generalized Gradient Approximation
HF	Hartree-Fock method
MOF	Metal-Organic Framework
MP2	Møller-Plesset Perturbation theory up to the 2^{nd} order
OTf	Trifluoromethanesulfonate ~ triflate
PAW	Projector Augmented Wave
PBE	Perdew-Burke-Ernzerhof functional
PES	Potential Energy Surface
T (atom)	tetrahedral atom in zeolite
TS	Transition State
vdW-DF2	second version of the van der Waals Density Functional
XRD	X-Ray Diffraction

1. Introduction

The theoretical investigation of reaction mechanism of Friedländer reaction, Knoevenagel reaction, and alcohol cyclization catalyzed by microporous materials is reported. Microporous materials and their use in catalysts are described in Section 1, together with a detail description of zeolite H-ZSM-5 and metal-organic framework (MOF) Cu_3BTC_2. An overview of possible applications of theoretical methods in catalysis research follows. Methods and models used to describe the catalysts investigated herein are presented in Section 2. Results are reported in Sections 3.1, 3.2, and 3.3 for Friedlander reaction, Knoevenagel reaction, and the intramolecular cyclization of alcohols, respectively. All results are finally summarized in Section 4.

1.1 Microporous Materials

Porous materials generally are one of the industrially most important groups of materials, with applications in adsorption, molecular sieving, catalysis, and other fields. They can be divided into three groups, depending on the diameter of pores: 1) macroporous materials with diameters greater than 50 nm (for example foams); 2) mesoporous materials with diameter between 50 and 2 nm (for example mesoporous silica) and 3) microporous with diameter of pores smaller than 2 nm. The applications of the porous materials are closely related to their pore diameter. Macroporous materials can be used as filters [1], supports [2] or adsorbents. The size of pores of meso- and microporous materials confines the possible sorbents to size of biomolecules or just simple chemical species, respectively. The mesoporous materials are thus used mostly as supports and catalysts [3–5]. The microporous materials are used in adsorption and catalysis [6–8].

Microporous materials constitute a wide group of materials, including porous nanocarbons, many types of porous metal oxides or some crystalline organic polymers. The most important group of microporous materials are zeolites. In recent years, novel materials called coordination polymers or metal-organic frameworks (MOF's) have also become vastly studied due to a large variety of structures and chemical compositions they offer. Both, zeolites and MOF's are studied herein and they are briefly described below.

1.1.1 Zeolites

Zeolites are crystalline aluminosilicates (based on SiO_2) with a three-dimensional framework structure that forms uniformly sized pores. The zeolites consist of SiO_4

tetrahedra linked to each other by shared oxygens. In some of these tetrahedra (generally called "T atoms"), the Si^{4+} atom can be replaced by heteroatoms, e.g., Al^{3+}, B^{3+}, Fe^{3+} that introduce the negative charge on the framework. The electroneutrality of zeolite is provided by extra-framework cations; most often by Na^{+}, K^{+}, Li^{+} or Ca^{2+} forming Lewis metal sites or by H^{+} forming Brønsted acidic sites. The concentration of non-Si atoms (commonly expressed as a ratio of Si/Al atoms in the zeolite) determines most of the zeolite properties as adsorbents and catalysts.

Depending on the type of the extra-framework atom the zeolites can be used as either acidic or basic catalysts [8]. The Brønsted acidity of zeolites depends mostly on the concentration of the H^{+} ions. The strongest H^{+} sites are present in the zeolites with higher Si/Al ration. In the case of basic zeolites the strength of Lewis basicity depends mainly on the nature of metal used as an extra-framework cation. Zeolites can be used also as redox catalyst, mainly after incorporating heteroatoms like Ti inside the framework [9].

The other factor playing major role in zeolite properties is the size and shape of the pores. Currently more than 200 zeolites are known, with pores as large as 18 T atoms (e.g. IRR or ETR zeolites; the size is determined by the number of T atoms enclosing the cut through the channel). Size and shape of channels limits the size of molecules, that are allowed to adsorb inside the zeolite and thus determines properties of zeolites as selective adsorbents and molecular sieves.

The zeolite structure and composition are determined by the synthesis conditions [10]. The zeolites are synthetized by dissolving the source of silica and alumina in a strong basic aqueous solution and subsequent long treatment in the autoclave. Formation of the particular type of zeolite and its properties are determined by a set of reaction conditions: 1) the ratio of alumina and silica source, 2) the basicity of the solution, 3) the nature of cation of the alkaline, 4) reaction conditions in the autoclave and 5) the structure directing agent. The structure directing agents (SDAs) are organic molecules that are leading the synthesis towards a particular zeolite; SDAs are usually quaternary ammonium salts [6]. Synthesis with SDAs is currently the most common type of synthesis of zeolites. It is nevertheless possible to carry out the synthesis without any SDA, as it is documented by the occurrence of natural zeolites.

Every synthetized zeolite structure type has three-letter code, assigned by the structure commission of the International Zeolite Association. Of about 200 synthetized types of the zeolitic frameworks, only 17 are commercially used. The largest amount of zeolites is used in the industry as additives in cement, release agents in agriculture or pH agents in aquaristic; these zeolites are mostly based on HEU and CHA types of frameworks. The LTA-type zeolites (NaA) are used as water softeners [6]. One of the

most valuable applications of zeolites is the catalysis, even though it is not the largest. The zeolites mostly used in catalysis include those based on FAU framework (zeolites X and Y), used in the oil refining in cracking processes [6]; other zeolites as the MFI- or BEA-type zeolites are used as additives for these processes.

The zeolite studied in this work is H-ZSM-5, MFI-type zeolite with Brønsted acidic groups. The ZSM-5 zeolite was first described by Kokotailo et al. in 1978 [11]. The MFI framework exhibits 3D system of channels, both of them with 10 member rings. One of the channels runs straight along the *b* lattice vector and the second one runs in a zig-zag manner in the *ac* plane (Figure 1.1).

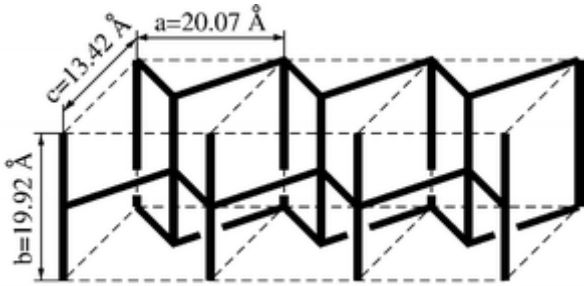

Figure 1.1 Scheme of the channel system inside the MFI structure: zig-zag channels running along *a* direction and straight channels running along *b* direction. The figure taken from Ref. [12]

ZSM-5 is one of the most important industrial catalysts, mainly in the form of Brønsted acid H-ZSM-5. It is used as the catalyst in the cracking processes during the oil refining. This process is used to produce ethylene and propylene from the higher hydrocarbons in oil; the ratio between ethylene and propylene is the state-of-art reaction and can be governed by the modification of the catalyst [13]. Both acidic and basic ZSM-5 zeolites have been also proven as the promising catalyst in the biomass refining into the chemicals [14] and biofuel [15,16]. ZSM-5 can be used to catalyse a variety of other reaction, for example the Cu and Fe doped forms of ZSM-5 can be used in the NOx reduction [17,18].

1.1.2 Metal-Organic Frameworks

Metal-organic frameworks are microporous materials that have been often investigated studied in last years. They can be described as coordination polymers in which various metal ions or clusters are interconnected by organic ligands (linkers) into the well-defined 3D frameworks (Figure 1.2). MOF's show large variability of structures; they can differ in structure type, organic linkers and the metal used [19]. The

resulting crystal structures often exhibit large porosity and internal surface that can even surpass that of zeolites; it can reach even the value of 6000 m^2 g^{-1} [20]. Even though the MOF's have been studied for variety of applications, they are not used in industry yet; mainly because of issues with long term and temperature stability.

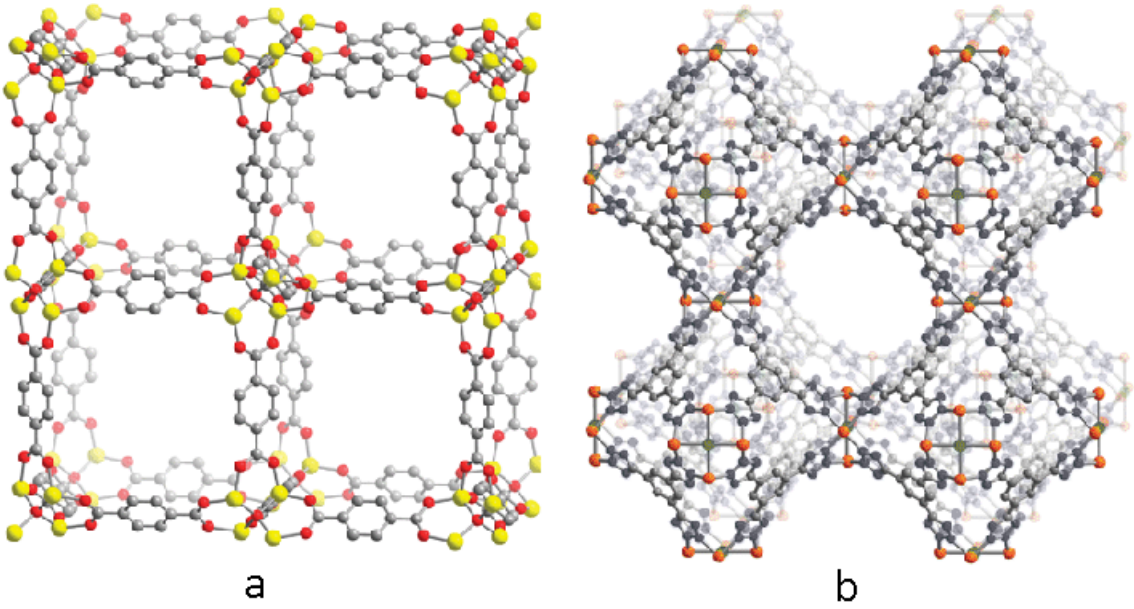

Figure 1.2 Examples of the MOF crystal structures, a – MOF-5 [$ZnO(BDC)_3$], (BDC stands for the benzene-1,4-dicarboxylic acid); b – $Mn_3[(Mn_4Cl)_3(BTT)_3]_2$ (BTT stands for the benzene-1,3,5-tris(1H-tetrazol))

There can be several types of metal sites in MOF's: i) metal oxide clusters that are connected to linkers via oxygen atoms, e.g. MOF-53 [21], ii) fully coordinated metal sites, e.g. ZIF-8 [22] and iii) partly coordinated metal sites, e.g. CuBTC [23]. The latter MOF's are of a large interest because they contain stable coordinatively unsaturated metal sites (*cus*). *Cus* sites in MOF's have interesting adsorption properties because they are preferential adsorption sites for the electrostatic interactions with, e.g., polar groups or double bonds and can be thus used for the separation of different types of molecules [24].

The applications of MOF's in catalysis is also of interest [25]. They can be used for reactions of bigger molecules than zeolites. There are different types of catalytic sites in MOF's (either on organic or on inorganic parts), including *cus* sites, that exhibit Lewis acid or even redox character [26]. Other types of catalytic sites are functional groups on linkers (like NH_2 groups [27] or functional groups immobilized on the framework [28]. The linkers can be also used to tune the electronic structure of the MOF to modify the Lewis acidity of *cus* sites [29]. Even MOF's having neither free metal sites nor functional groups have been reported to catalyse some organic reactions [30]. This is

commonly explained by the presence of defects in framework structure, mostly broken metal-oxygen bonds, and presence of Brønsted OH group catalysing the reaction [26].

A novel application of MOF's as bifunctional catalysts has been reported recently [31]. Two different types of multifunctional MOF's can be considered; i) structures with two types of metal sites and ii) structures containing both *cus* sites and functionalized linkers. Catalysts with various metal site types can be created, e.g., by doping of Pd or Pt inside the framework; such frameworks were found active in catalysis of arylamines or quinolines [32], heteroannulation reactions [33] or carbonyl condensation [34]. The MOF's containing both *cus* and functionalized linker have a large variety of possible active groups; however, mostly amino- functionalized MOF's are used, for example in aldol condensation [31] or Knoevenagel condensation [35,36].

The HKUST-1 MOF [23] (often denoted as CuBTC) is studied in this work. The basic structure units of this MOF are Cu^{II} atoms linked by the BTC linker (benzene-1,3,5-tricarboxylic acid) into the network with the chemical formula [Cu_3BTC_2] (Figure 1.3). The structure of CuBTC exhibits two types of interconnected cages with diameters of 9 Å and 6 Å. All Cu^{2+} ions form *cus* sites with the free coordination site accessible from the 9Å cage (they are inaccessible from the 6Å cage); there are twelve *cus* sites accessible from each suppercage. The internal surface of CuBTC can reach the value of 2000 $m^2\ g^{-1}$ and density of 0.35 g cm^{-3}; however, the actual surface depends on the method of sample preparation [37]. The real values of the internal surface vary between 900 and 2200 $m^2\ g^{-1}$. The CuBTC is one of a few commercially available MOF's denoted Basolite C300 (the internal surface of 1600 $m^2\ g^{-1}$).

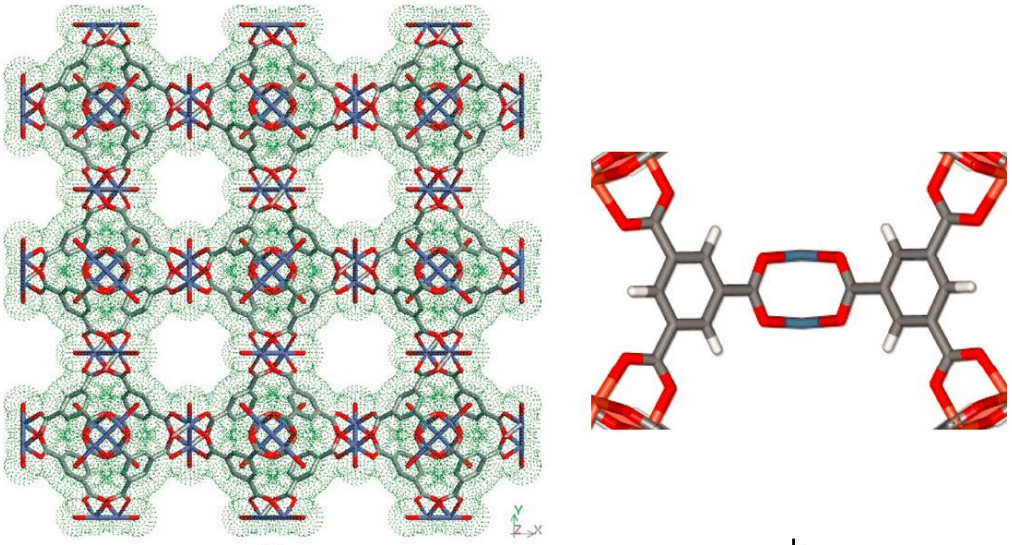

Figure 1.3 a – The crystal structure of CuBTC, with waters coordinated on *cus* sites, hydrogens are omitted for simplicity, b – the surrounding of *cus* sites. The blue, red, grey and white colours are used for the Cu, O, C and H atoms, respectively

The CuBTC can be synthetized by the direct reaction of the Cu^{2+} source (mostly $Cu(NO_3)_2$) with BTC acid under high temperature. In the as-synthetized state all *cus* sites in MOF are occupied by water molecules. The water can be completely removed by thermal treatment at 350 – 400 K [38] (the thermal stability of CuBTC is about 550 K). It was shown that CuBTC has a properties of a hard Lewis acid, thus confirming that *cus* sites play a major role in catalysis [39]. CuBTC has potential applications in adsorption, for example in separation of tetrahydrothiophene (odorant of natural gas) [40], and in catalysis, where it was proven to be efficient catalyst of reactions like oxidation of polyphenols, cyclization of citronellal, and cyanosilylation or isomerization of α-pinen oxide [41].

1.2 Theoretical investigation of microporous materials

The computer development in last decades has allowed using models and methods that can reasonably well describe even complex systems. Computational methods can be divided into two main types; classical and quantum calculations. Classical methods can be used to describe the motion and properties of particles based on the classical physics formalism, but they neglect the details of electronic structure. All the calculations reported herein are based on the quantum mechanical description of the system that is used for the description of the microporous materials and in the investigation of reaction mechanisms.

Computational chemistry is a useful tool for the investigation of processes inside microporous materials. The microporous materials investigated herein are crystalline materials with well-defined structures and, thus, they can be described with a rather good accuracy. The quantum chemical methods are computationally too expensive for the description of entire crystals of the material. However, the simplified models can be introduced, describing only the important part of the system. Generally, two types of models can be used; i) periodic models, simulating crystal unit cell and assuming the infinite number of repetitions in all three directions and ii) cluster models of the particular active sites.

Both types of models have their pros and cons. The periodic models simulate all atoms inside the ideal crystal of the material. Due to the large size of unit cells of many zeolites and MOF's, the most precise *ab initio* methods cannot be used. The currently most common compromise between the cost and the accuracy is the use of DFT methods; mainly semi-local generalized gradient approximation (GGA) functionals [42] are used. These functionals underestimate the interaction of molecules with the framework, mainly due to the inability to describe dispersion interactions between adsorbates and adsorbents. This is a significant problem for microporous materials since an important part of the interaction energy with is due to the dispersion interactions. Currently there are two methods how to overcome this problem, either using semi-empirical correction [43] or using the non-local vdW density functionals [44].

More accurate methods, including *ab initio* post Hartree-Fock (HF) methods as Coupled Clusters, can be used for cluster models. The disadvantage of cluster models is the incomplete description of the material. However, cluster models can be used for accurate analysis of interactions and for benchmarking of DFT-based methods. This has a great importance in MOF's, in structures with *cus* sites particularly, because DFT methods are often inaccurate when describing the electronic structure of transition metal sites.

Theoretical methods have been widely used for the description of the zeolites and MOF's properties. They helped in the determination of structures of some more complicated MOF structures, e.g., UiO-66 [45]. The main role of calculations is in the description of the active site though. The probing of the nature and strength of both Brønsted and Lewis sites in zeolites has been a common task of computational methods; for example by modelling of CO adsorption and interpreting the experimental FTIR [46,47], or by the investigation of the adsorption and reactivity of bigger molecules like isobutene [48]. The significance of synergy between experiment and theory is even bigger in MOF's. Theoretical calculations can probe every type of adsorption or active sites on the molecular level, thus, they can be used for description of either one

particular site or the description of all effects from the framework. The example can be CuBTC, in which the adsorption of small molecules was theoretically studied by Chen et al; the authors characterized all adsorption sites of CH_4 in CuBTC and showed the complete description of its adsorption mechanism in this material [49].

The investigation of reaction mechanisms is the second task investigated herein. The principle of determination of the reaction mechanism is the localization of the reaction coordinate on the potential energy surface (PES). The minima on the resulting reaction path represent the reaction intermediates and the saddle points of the first order are the transition structures (the activated complexes). Only less precise methods can be used for the investigation of more complex reactions because lots of geometry optimizations have to be used for the search of transition states. The more precise post-HF methods are thus used scarcely in this field, or only to correct the energy values obtained with cheaper methods; the hybrid DFT methods (like B3LYP [50,51]) are applied in this field most often [52,53].

The selection of the right model is the main issue in the investigation of reaction mechanism in microporous materials. Due to the computational expenses the use of periodic models in transition state structure search is limited. The optimal scheme for the localization of transition states is thus the use of periodic model calculations for the localization of intermediates and subsequent localization of transition states with the cluster models.

A variety of reactions catalyzed by microporous materials has been studied by computational methods. Reactions running on zeolites have been studied already in 1990’s for the reactions like methanol condensation [54] or isomerisation of alkenes [55], but all of them used very small cluster models of zeolites (clusters consisting of 1 or 3 tetrahedra, co called 1-T or 3-T cluster models). However, in recent years, more precise calculations with bigger models of catalyst allowed investigation of many mechanisms for even more complex reactions; like simultaneous reduction of aldehydes and oxidation of alcohols [56] or ethylation of benzene [57]. On the other side, only few mechanisms of reactions catalyzed by MOF's have been computationally investigated yet; for example cyclization of citronellal in UiO-66 [29], Knoevenagel reaction in IRMOF-3 [58] or trans-esterification reaction on ZIF-8 [59].

2. Methods and Models

2.1 Periodic models

Two different microporous catalysts are studied in this work: the CuBTC metal-organic framework and the H-ZSM-5 acidic zeolite. To enable modelling of reactions in these systems, two types of simplified models has been used; i) periodic models, simulating crystal unit cell and assuming the infinite number of repetitions in all three directions, and ii) cluster models of the particular active sites.

The CuBTC is described first (Figure 2.1); it is represented by a rhombohedral primitive cell, with cell parameters optimized previously (a = b = c = 181.774 Å and $\alpha = \beta = \gamma = 60°$, volume 4678.71 Å^3) [60]. The primitive cell contains 156 framework atoms, of which 12, 48, 72 and 24 are Cu^{2+} ions, O, C and H atoms, respectively.

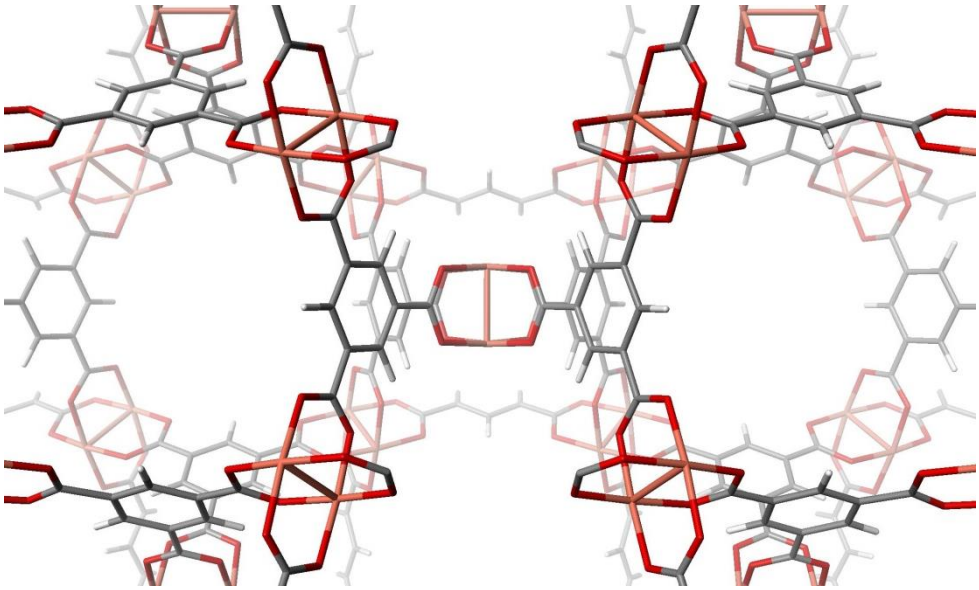

Figure 2.1 Structure of CuBTC metal organic framework. Colouring scheme: H, C, O and Ge atoms depicted in white, grey, red and pink colours, respectively

The MFI unit cell optimized previously for purely siliceous system containing 96 and 192 Si and O atoms, respectively, was used (parameters a = 20.241 Å, b = 20.001 Å and c = 13.514 Å, $\alpha = \beta = \gamma = 90°$, volume 5471.0 Å^3) [61]. To model a Brønsted acid site, Si in T12 position (at the intersection of main and zig-zag channels) was substituted by Al atom and the negative charge was compensated by H^+ (Figure 2.2). The second Al atom was substituted into T1 position, just across the channel intersection from the first Brønsted site.

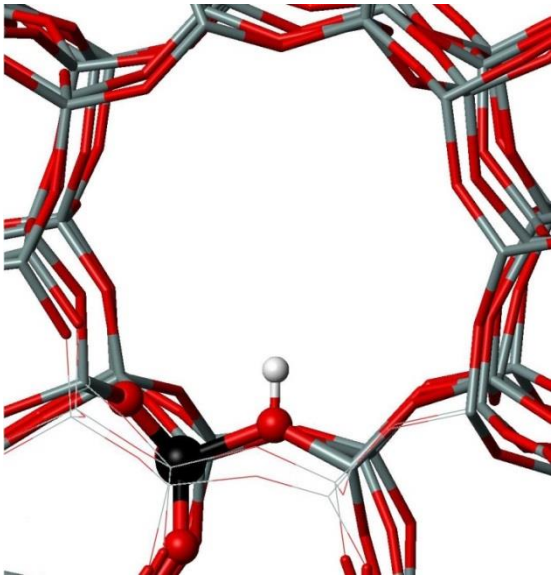

Figure 2.2 The Brønsted acidic site pointing in the straight channel of MFI structure, the framework Si, Al, and O atoms are depicted in grey, black and red colour, the Brønsted H atom is shown in white.

DFT methods were used in all calculations with periodic models, either with PBE exchange-correlation functional [62] or with the second version of the non-local van den Waals density functional vdW-DF2 [63] which accounts for dispersion interactions. The projector augmented wave (PAW) [64] and plane-wave basis set with the kinetic energy cutoff of either 400 or 600 eV were used, together with the Γ-point sampling of the first Brillouin zone. All periodic DFT calculations were performed with the VASP program package, version 5.2.12 [65,66]. The methods used are specified in Models and Methods subsections for particular reactions.

2.2 Cluster models

For the investigation of reaction mechanisms, various cluster models were used. Only the active site and its close surrounding were explicitly considered in the cluster models. For simulation of Brønsted acid sites in H-ZSM-5, so called 3-T cluster model with empirical formula $Si_2AlO_4H_9$ was used (Figure 2.3); T stands for one tetrahedral atom of zeolite (Si or Al). The cluster is OH–terminated on Al atom while it is just H-terminated on Si atoms to avoid an artificial interaction of reactants with the cluster-terminating silanol groups.

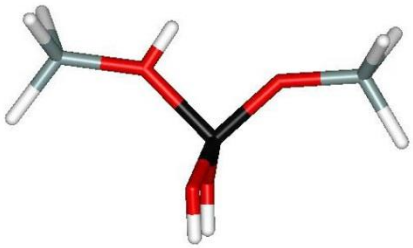

Figure 2.3 3-T cluster model of the Brønsted acid site inside a zeolite

The *cus* sites in CuBTC are formed by the Cu^{2+} ions surrounded by four oxygens in the slightly pyramidal geometry (O–Cu–O angle of 173.9°) with Cu pointing towards the cage (Figure 2.1). The simplest representation of the *cus* site is a cluster formed by two Cu^{2+} ions connected via four carboxylic groups (Figure 2.4a). The $Cu_2(HCOO)_4$ cluster model is used and it is denoted as "paddlewheel". For the sake of computational feasibility a small $Cu(HCOO)_2$ cluster model was also employed (Figure 2.4b). Cluster model calculations considering the interaction with just one active site (represented by a $Cu(HCOO)_2$ model) are referred to as **single-site** cluster model calculations. For the investigation of simultaneous interaction of reaction intermediate with two active sites a **two-site** cluster model was introduced; it consists of a pair of $Cu(HCOO)_2$ cluster models at geometry corresponding to the CuBTC MOF (Figure 2.5a). The distance between two Cu^{2+} sites is thus 8.15 Å.

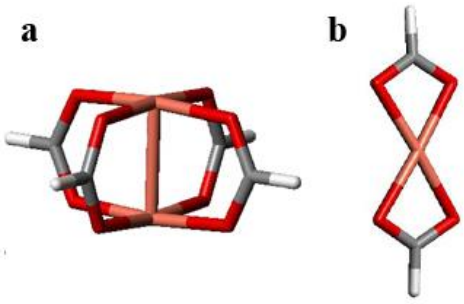

Figure 2.4 Small cluster model of the CuBTC; a – paddlewheel cluster, b – $Cu(HCOO)_2$ cluster

The **two-site** cluster model consisting of two paddlewheel clusters linked by one benzene (Figure 2.5b) was also used in the Knoevenagel reaction study ($Cu_2(HCOO)_3(OOC–C_6H_4–COO)(HCOO)_3Cu_2$ and it is denoted **two-pdw** model). Only the geometry of some atoms in the cluster was constrained in the geometry optimization (depicted as thinner tubes in Figure 2.5b); however, the closest surroundings of active sites was fully relaxed.

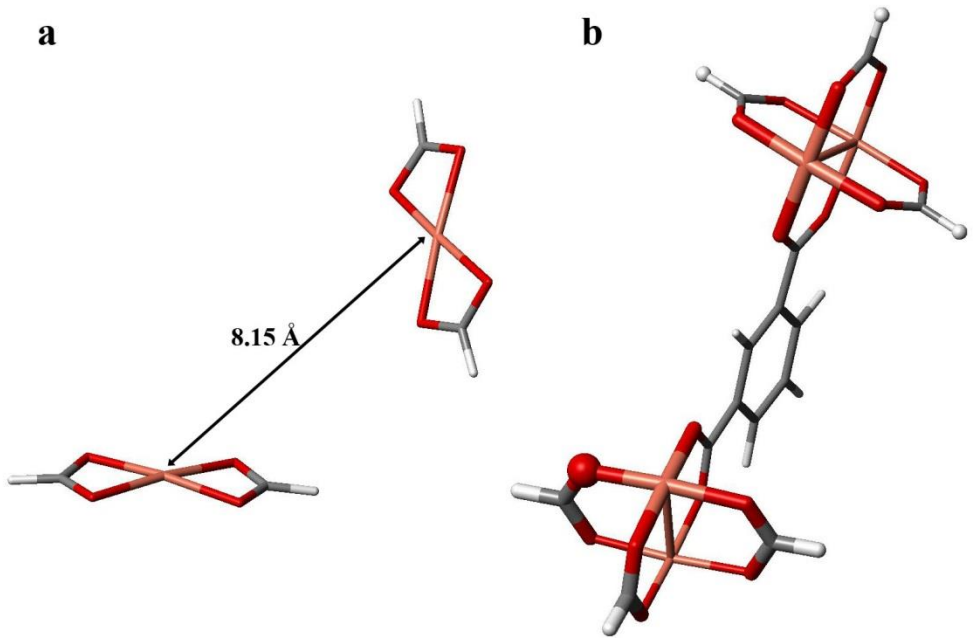

Figure 2.5 a – **two-site** model of CuBTC consisting of two $Cu(HCOO)_2$ clusters; b – **two-pdw** model consisting of two paddlewheels connected by one benzene ring, thinner tubes denote frozen parts of the cluster, oxygen depicted by the sphere is the oxygen on which the defect is formed.

Calculations with all cluster models were performed with the Gaussian 09 program suite [67]. The reaction mechanisms of all reactions were investigated with Becke's three parameter exchange–correlation functional B3LYP [50,51]. To compare the cluster and periodic model calculations the PBE exchange-correlation functional was also used [62]. In cases where more accurate calculations were required, Møller–Plesset perturbation theory through the second order (MP2) was used. Basis sets used with DFT functionals were either Pople type basis sets 6-311G(2d,p) and 6-311G(d,p) [68] or correlation-consistent basis set cc-pVTZ [69]. The character of all stationary points located along the reaction paths was checked by the frequency calculations performed within the harmonic approximation. The system-specific details are specified in Models and Methods subsections for particular reactions.

3. Theoretical investigation of selected reactions

3.1 Friedländer reaction

In this section, explanation of catalytic activity of CuBTC in the Friedländer reaction is reported. Friedländer reaction is a double condensation of *o*-aminoaryl carbonyl molecules with other carbonyl compounds with enolizable hydrogens. It is considered to be economic way to produce substituted quinoline compounds [70]. These N containing heterocyclic compound are frequently used in medicine as antimalaric drugs [71] or it can be used as anti-inflammatory [72] or anti-asthmatical [73] drugs. Other uses of quinolines include dyes, novel materials or electronics [74].

For the catalysis of Friedländer reaction, both bases and acids can be used [75]. The reaction can be even run without catalyst for some reactants using temperatures between 150 – 220 °C. The most common is the catalysis by strong inorganic or organic base at high temperature in water or alcoholic solution; e. g., ytterbium triflate $Y(OTf)_3$ [76]. Other salts such as BCl_3 [67] or $SnCl_2$ [77] can be also used.

Some microporous materials have been already tested as catalysts for the Friedländer reaction, with reactants shown in Figure 3.1. Acidic zeolites as H-FAU, H-MOR or H-BEA have proved to be quite efficient catalysts [78] with conversions higher than 50 % over 6 h. However neither of these zeolites was selective exclusively for the Friedländer reaction products. The CuBTC MOF has been also tested as catalyst and it turned out to be more efficient than zeolites with quantitative conversion in 3 h at 100 °C with the 100% selectivity for Friedländer products [79]. The CuBTC was further investigated to explain such high activity [80]. The catalytic activity of CuBTC was attributed to Cu ions; even the Cu containing zeolite BEA (proven before to be the best among zeolites) had lower activity than of CuBTC. This indicates that the activity of CuBTC comes from some specifict feateure of its structure.

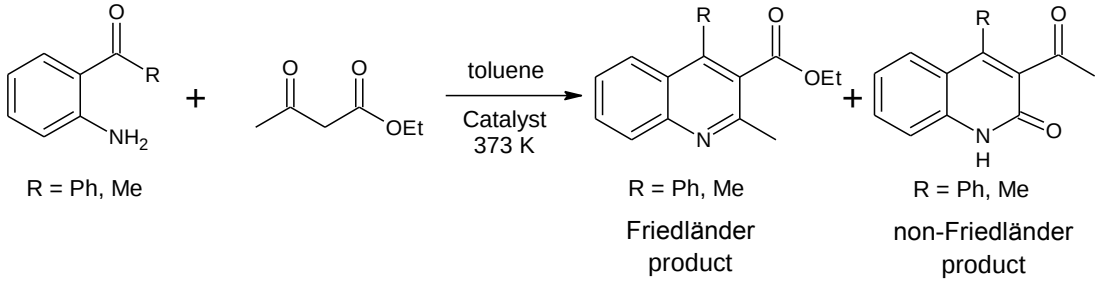

Figure 3.1 Friedländer reaction used in the catalytic testing of zeolites and CuBTC [78–80]

The Friedländer reaction has been already investigated in my Bachelor thesis [81]; in particular the reaction mechanism for uncatalyzed reaction, reaction catalyzed by H^+ (as a Brønsted acid) and reaction catalyzed by CuBTC (as a Lewis acid) represented by a **single-site** cluster was studied. The results reported in Bachelor thesis are briefly summarized below, followed by a detail description of new results obtained during the course of my Master thesis.

Two possible pathways were found for the reaction of 2-aminobenzaldehyde **F1** and acetaldehyde **F2**, differing in the order of elementary reaction steps (Figure 3.2): i) reaction starting with aldolization (**F1**+**F2e** → **F3a**) following by subsequent C–N formation (**F3a** → **F4a**) and two dehydrations; ii) reaction starting with imination (**F1+F2** → **F3i** → **F4i**) followed by the aldolization **(F4i** → **F5**) and dehydration. The preference for particular reaction path was found to depend on the type of catalyst used in the reaction. The aldolization path is preferred in uncatalyzed reaction. On the contrary, the imination reaction path is preferred in the reaction catalyzed by the Brønsted acid.

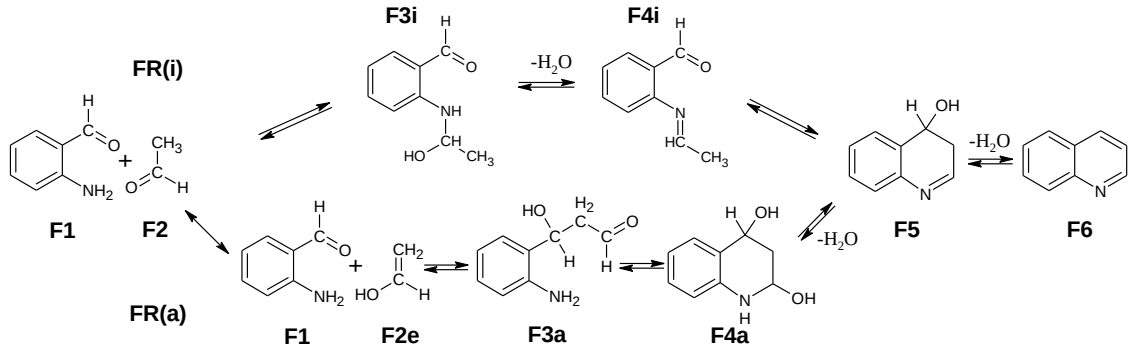

Figure 3.2 The reaction mechanism of the Friedländer reaction; the upper and lower parts of the scheme show reaction starting with imination **FR(i)** and aldolization **FR(a)**, respectively.

The catalytic activity of CuBTC (Lewis acid) was investigated using a **single-site** model represented by a $Cu(HCOO)_2$ cluster (see section 2.2). It was found that there are two different reaction paths depending on the reactant-catalyst interaction mode; either

via oxygen (O-down) or nitrogen (N-down) of aminobenzaldehyde **F1**. Reaction precursors for both paths are energetically almost identical; however the stationary point geometries are rather different. It was found that the copper catalyst leads to the reduction of the overall barrier of the aldolization reaction path only; the C–C and C–N formation steps in particular, while dehydration steps remains unchanged.

The mechanism of Friedländer reaction catalyzed by CuBTC has been re-investigated using a better model of catalyst and the results are reported below. The motivation for the model improvement is based on the hypothesis that intermediates can interact with more than one catalytic site inside CuBTC simultaneously (Figure 3.3) and that could lead to a change of the reaction mechanism. Part of these results was already published in Dalton Transactions [82].

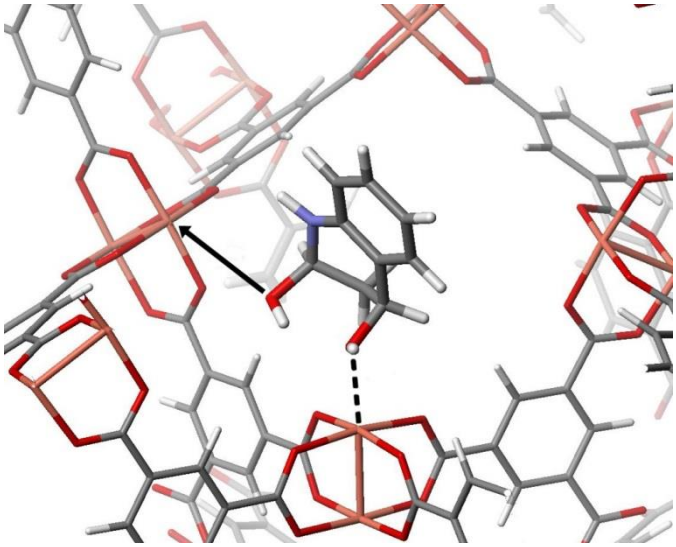

Figure 3.3 Intermediate **F4a** interacting with the CuBTC, dashed line shows strong interaction with *cus* site, arrow shows weaker interaction with secondary active site

3.1.1 Methods and Models

2-aminobenzaldehyde **F1** and acetaldehyde **F2** were chosen as the model reactants. Reaction path is depicted in Figure 3.2; the **FR(a)** mechanism with the O-down reaction precursor is considered. The reaction was investigated using **two-site** model (see Chapter 2.2) with B3LYP functional and 6-311G(2d,p) basis set. To verify the model, minima on reaction paths were also investigated using periodic model of CuBTC and PBE functional and energy cut-off of 600 eV (see Chapter 2.1). To allow comparison of cluster and periodic calculations, energies of minima on reaction path were recalculated with PBE functional and 6-311G(2d,p) basis set.

3.1.2 Results

The relative energies (with respect to reactants **F1** and **F2** interacting with the model catalyst) of all minima along the **FR(a)** reaction path in O-down interaction mode obtained with **single-** and **two-site** cluster models and the periodic model of catalyst are summarized in Table 3.1. The discrepancy between the **single-site** cluster model and the periodic CuBTC model increases along the reaction path. The **two-site** model introduced herein gives the results in a very good agreement with the periodic CuBTC model.

Table 3.1 Relative energies of minima in **FR(a)** mechanism calculated with various models of catalyst (in kJ mol^{-1})

Structure	Model		
	single-site	**two-site**	CuBTC
F1+F2	0	0	0
F1+F2e	42	46	51
F3a	45	73	72
F4a	-30	4	6
F5	15	11	1
F6	-35	-63	-73

[a] PBE functional used; relative energies reported with respect to the energy of interacting reactants and the model catalyst (**F1+F2**)

The reaction profile of **FR(a)** path obtained with the **two-site** cluster model is shown in Figure 3.4 and corresponding barriers are summarized in Table 3.2. Neither aldolization nor C−N formation steps are affected by the secondary catalytic site, except for the stabilization of reactants due to the interaction of **F2** with the secondary Cu^{2+} site. However, the rate determining step (dehydration **F4a→F5**) is significantly–influenced by the presence of the secondary catalytic site; relative energy of corresponding TS decreases by 42 kJ mol^{-1}. Apparent activation barriers of both dehydration steps are almost 100 kJ mol^{-1} lower than for uncatalyzed process (Table 3.2).

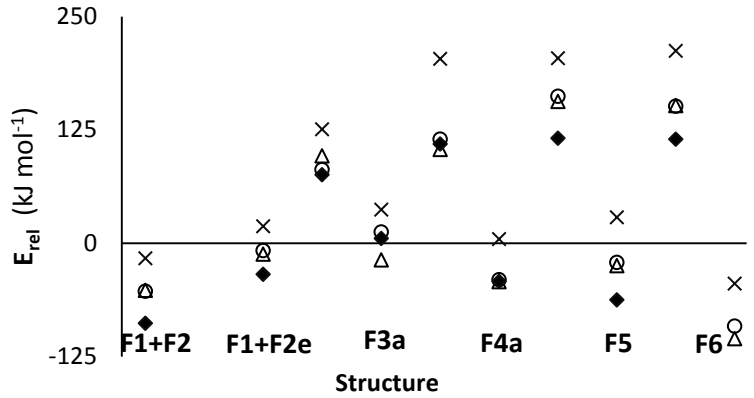

Figure 3.4 Energy profiles of FR(a) reaction path for uncatalyzed reaction and reaction catalyzed with one or two active sites; both O-down and N-down intermediates are considered. The x-axis represents a reaction coordinate; the notation introduced in Figure 3.2 is adopted. All energies were calculated using B3LYP functional. (X) Uncatalyzed, (Δ) **single-site**/N-down, (○) **single-site**/O-down, (♦) **two-site**/O-down, structures 5 and 6 are reported for N-down for which the activation barrier is lower

Table 3.2 Reaction profiles of **FR(a)** mechanism obtained with various models [82].[a]

Structure	Uncatalyzed		**single-site**/N-Down		**single-site**/O-Down		**Two-site**	
	E_{rel}	$E^{\neq}$	E_{rel}	$E^{\neq}$	E_{rel}	$E^{\neq}$	E_{rel}	$E^{\neq}$
F1+F2	-16.8		-52.2		-53.1		-88.5	
F1+F2e	18.3		-12.2		-8.4		-34.4	
TS **F1+F2e →F3a**	125.3	107.0	96.0	108.2	81.0	89.5	75.5	109.9
F3a	36.7		-18.7		12.2		4.9	
TS **F3a→F4a**	203.0	166.3	103.2	121.9	114.4	102.3	109.1	104.2
F4a	4.2		-42.6		-40.5		-42.3	
TS **F4a→F5**	203.8	199.6	156.3	198.9	161.8	202.2	115.7	158.0
F5	28.5		-25.0		-21.6		-62.9	
TS **F5→F6**	212.0	183.6	151.7	176.7	150.8	172.4	114.5	177.4
F6	-44.7		-105.6		-91.7		-148.4	

[a] Relative energies E_{rel} with respect to the energy of non-interacting reactants and catalyst and activation energies for elementary steps $E^{\neq}$ are reported in kJ mol^{-1}; results obtained with B3LYP functional reported.

The effect of the secondary catalytic site on the dehydration steps is shown in Figure 3.5. On the **single-site** model of catalyst, water leaves **F4a** intermediate without any stabilization (Figure 3.5a). Similar TS can be found with the **two-site** cluster model, in which water leaves **F4a** without interaction with the secondary active site (Figure 3.5b). Nevertheless, the interaction of **F4a** with two Cu^{2+} sites results in the lowering of TS energy by 18 kJ mol^{-1}. In addition, the dehydration can follow the path through the

transition state depicted in Figure 3.5c; **F4a** interacts only with the primary active site and dehydrated water interacts with the secondary active site. The barrier for this elementary step is 42 kJ mol^{-1} lower than for the corresponding reaction step catalyzed by the single catalytic site.

The barrier of the second dehydration step does not change significantly because the distance between nitrogen and OH group is too small to allow simultaneous adsorption on two *cus* sites. The leaving OH group thus interacts only with the water formed in the previous reaction step.

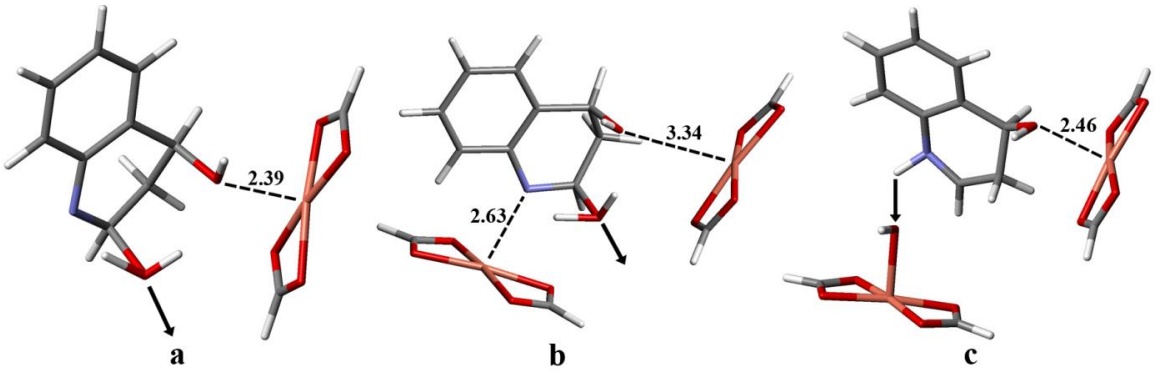

Figure 3.5 Structures of transition states for the first dehydration step (**F4a→F5)** in **FR(a)** mechanism obtained with the **single-site** (a) and the **two-site** (b, c) cluster models. Concerted effect without and with stabilizing interaction of dehydrated water with the secondary Cu^{2+} site is depicted in parts b and c, respectively. Solid arrows represent a dominant component of reaction coordinate; distances in Å.

3.1.3 Discussion

Results reported previously for the **single-site** model [81] indicated that out of the four-step reaction mechanism (**FR(a)** in the Figure 3.2) only the first two steps are effectively catalyzed; contrary to experimental results [79,80] that had showed high activity of CuBTC in the reaction. It was proposed that the catalytic activity of CuBTC could be explained by the adsorption simultaneously on the two neighbouring active sites that are only about 8.1 Å apart in CuBTC (Figure 3.3). The role of the secondary catalytic site has been investigated in detail herein.

The results show the activity of the catalyst is significantly increased due to the concerted effect of two adjacent active sites. While the structures of reaction intermediates remain similar as in the reaction catalyzed by one active site, the relative energies are changed significantly. C−N formation and aldolization steps are not influenced by the secondary catalytic site; however, the activation barriers of other

reactions steps, in particular dehydration reactions are reduced due to the simultaneous interaction of reaction intermediates with a pair of adjacent catalytic sites (Table 3.2).

The activation barrier of the rate determining step (dehydration) of the **FR(a)** reaction path is significantly reduced due to the concerted effect of two nearby Cu^{2+} sites. The activation barrier of this reaction is reduced to 116 kJ mol^{-1} that is about half of the barrier found for uncatalyzed reaction (212 kJ mol^{-1}). It is reasonable to anticipate that the barrier will be even lower when larger reactant (than a model acetaldehyde **F2** investigated here for computational reasons) is considered. Thus the results confirm that the **FR(a)** is the actual reaction path of the Friedländer reaction on CuBTC.

Note that the activation barrier for the second dehydration step **F5** → **F6** is lower for the N-down geometry (contrary to other reaction steps). It is reasonable to assume that all reaction intermediates can desorb and re-adsorb during the course reaction because adsorption energies of all intermediates are about half of the values calculated for activation barriers.

The simultaneous interaction of molecules with multiple active sites is not a commonly considered phenomenon in MOF's; however, it has already been reported for adsorption and catalysis in zeolites [83,84]. In general, a simultaneous interaction of reactants (or reaction intermediates) with two or more adsorption sites can either lead either to an increase of the catalytic activity or to the decrease of catalytic activity (when a strong interaction of reactant with multiple active sites makes the adsorption complexes too stable, see Section 3.3 for an example). The positive effect reported above Friedländer reaction. The concerted effect of two adjacent Cu^{2+} sites proposed above for Friedländer reaction catalyzed by CuBTC is novel phenomenon for MOF's. The principle is very similar to another possible usage of MOF's in catalysis – as bifunctional catalysts (see chapter 1.1.2), i.e. as catalysts with synergic effect of metal site and functional group on linker. However, to the best of our knowledge, no other synergic catalytic effect of two adjacent metal sites in MOF has been proposed yet.

3.2 Knoevenagel reaction

The mechanism of Knoevenagel reaction catalyzed by CuBTC is reported in this section; this investigation is focused on the interpretation of the recent experimental work [85]. Knoevenagel reaction is a standard procedure for the creation of new carbon-carbon bonds. It is a reaction of carbonyls with active-methylene compounds. It is very versatile reaction, used for example in the synthesis of fine chemicals or biologically active molecules [86,87]. The reaction mechanism of Knoevenagel reaction catalyzed by stronger bases is shown in Figure 3.6 (the mechanism is shown for reaction of malononitrile with benzaldehyde used in this study). Reaction starts with the methylene deprotonation [88], followed by the C–C bond is creation. Thus formed intermediate is then protonated again and subsequently dehydrated. However, other mechanisms can take place on different catalysts. When catalyzed by amino groups, the active methylene compound is first transformed to imine intermediate [89]. The Lewis acids, on the other side, activate the aldehyde, which then reacts directly with active methylene [90].

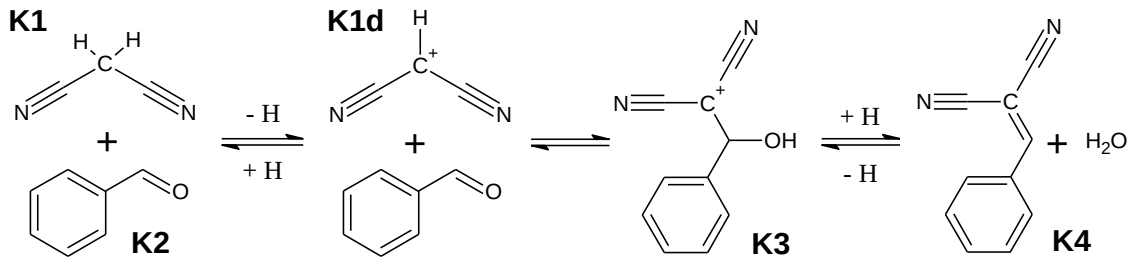

Figure 3.6 Reaction scheme of Knoevenagel condensation of malononitrile with benzaldehyde

The most common catalysts for the Knoevenagel reaction are inorganic bases or amines; the Knoevenagel reaction can be also used for the determination basicity of catalysts [88,91]. A variety of heterogeneous catalysts can be used for the Knoevenagel reaction, including hydrotalcites [92], clays [93] or functionalized silica [94]. However the best results were obtained with functionalized mesoporous silica and microporous materials. MCM-41 grafted with amines [95] or Schiff base [96] and basic zeolites [88,97] were found to be efficient catalysts for this reaction. Recently, variety of MOF's has been tested as catalysts for condensation reactions and particularly Knoevenagel reaction, with results summarized in recent review by Dhakshinamoorthy et al. [98]. Among others notable results, very high activity has been reported for some amino-substituted MOF's that could be possibly attributed to the concerted effect of NH_2 substituents and metal active sites inside MOF's; amino-groups and defects in crystal structure in IRMOF-3 [58] [27,99] or free metal sites in Fe-MIL-101-NH_2 [100].

The CuBTC was also recently reported to be efficient catalyst in the work by Opanasenko et al. [85]. The Knoevenagel reaction of benzaldehyde or cyclohexane carbaldehyde with ethyl acetoacetate, methyl cyanoacetate and malononitrile was tested. An excellent catalytic activity of CuBTC was demonstrated, often surpassing activity of acidic zeolites tested in the same reactions. The best activity was found for the reaction of benzaldehyde with malononitrile giving the 100% conversion in less than 1 h even at temperatures where zeolites were not active at all. Such activity highly surpasses the expectation for Lewis acid. It was shown that the CuBTC retains its structure (no XRD changes) and activity during the reaction. The aim of this theoretical study is to find the mechanism of the Knoevenagel reaction in the CuBTC and to determine the effects responsible for the efficiency of this catalyst.

3.2.1 Methods and Models

The mechanism of Knoevenagel reaction was investigated for the condensation of the malononitrile **K1** and benzaldehyde **K2**; the reaction scheme is depicted in Figure 3.6. Interactions of reactants with the catalyst were investigated using **single-site** and **two-site** cluster models (see Chapter 2.2) at the B3LYP/cc-pVTZ and MP2/cc-pVTZ level of theory. In addition, the cluster model consisting of two paddlewheels bridged clusters connected by one benzene unit was used (Figure 2.5b, Chapter 2.2). These calculations were performed with B3LYP functional and 6-311G(2d,p) basis set and compared with periodic model calculations performed with vdW-DF2 functional and kinetic energy cutoff 600 eV. For further description see Section 2.

3.2.2 Results

In analogy with the previous investigation of mechanism of the Friedländer reaction, a possibility of the interaction of reactants with two active sites simultaneously was tested. The interaction energies obtained with **single-site** and a **two-site** cluster models are summarized in Table 3.3. It was found that malononitrile **K1** can interact with two active sites simultaneously (Figure 3.7a); such adsorption complex is characterized by interaction energy that is twice as large as the one for adsorption complex formed on single adsorption site Table 3.3. On the contrary, interaction of benzaldehyde is not much affected by the presence of a secondary active site.

Table 3.3 Interaction energies (in kJ mol^{-1}) of reactants in Knoevenagel reaction with **single-site** and **two-site** cluster models.[a]

Structure	Method	Model	
		single-site	two-site
K1	B3LYP	-16.7	-27.1
	MP2	-31.2	-55.5
K2	B3LYP	-25.1	-26.0
	MP2	-40.5	-47.6

[a] cc-pVTZ basis used; all energies corrected for BSSE

It is reasonable to assume that Knoevenagel reaction starts by deprotonation of malononitrile (**K1d** formation). Such process however requires a Brønsted base; neither the reactants nor the CuBTC catalysts can act as a Brønsted base (see beginning of section 3.2). Therefore, a possibility of dynamic creation of Brønsted base during the course of the reaction was considered. Malononitrile interacts strongly with the Cu^{2+} cations in paddlewheel unit and the interaction of Cu^{2+} with carboxylic groups of organic linkers becomes weaker. Consequently, one of the four carboxylic groups forming paddlewheel unit can accept proton (acting as a Brønsted base). Structure of such intermediate is depicted in Figure 3.7b; the Cu^{2+} cation is coordinated to three carboxylic groups and to CN group of deprotonated malononitrile (Cu–N bond length of 1.86 Å) and carboxylic acid is formed. The charge balance on paddlewheel unit is then provided by deprotonated malononitrile and three carboxylic groups. The mechanism of Knoevenagel reaction catalyzed by CuBTC is divided into two parts: (i) the transfer of H^+ from malononitrile to carboxylic group and (ii) a Knoevenagel condensation itself.

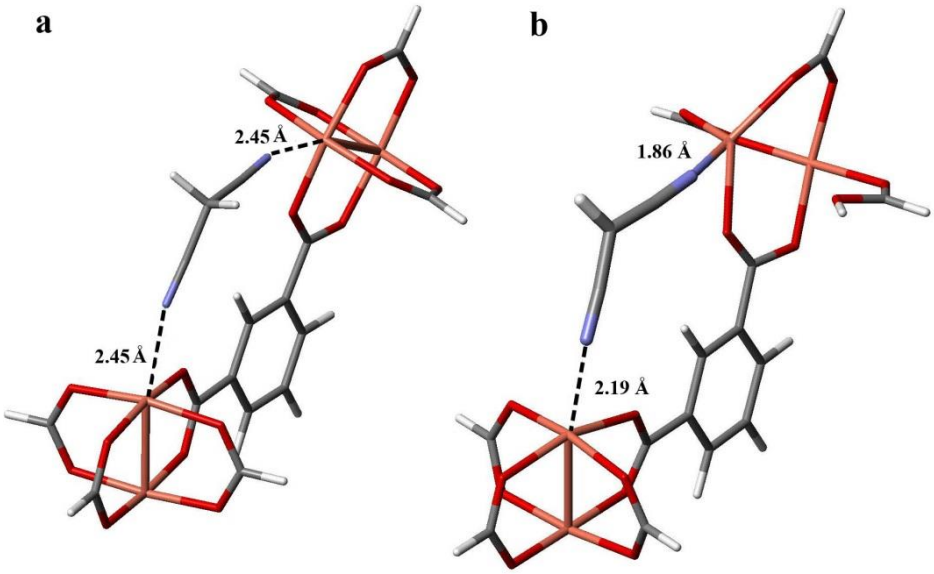

Figure 3.7 a – neutral malononitrile **K1** adsorbed to the **two-pdw** cluster; b - Deprotonated malononitrile **K1d** adsorbed to the **two-pdw** cluster with the defect on one of Cu–O groups, formed by H^+ from the malononitrile

The transfer of H^+ directly from the malononitrile to carboxylic group was found to be connected with large activation barrier. However, this process can be mediated (autocalyzed) by the benzaldehyde molecule; a two-step mechanism is shown in Figure 3.8. A protonated benzaldehyde is formed first (**K5**). Thus formed deprotonated malononitrile significantly increases its interaction with the Cu^{2+} site while the strength of the interaction of one carboxylic group with the paddlewheel becomes weaker. The proton is subsequently transferred to this carboxylic group, benzaldehyde is released and **K1d** intermediate is formed. This reaction step is about 72 kJ mol^{-1} endothermic.

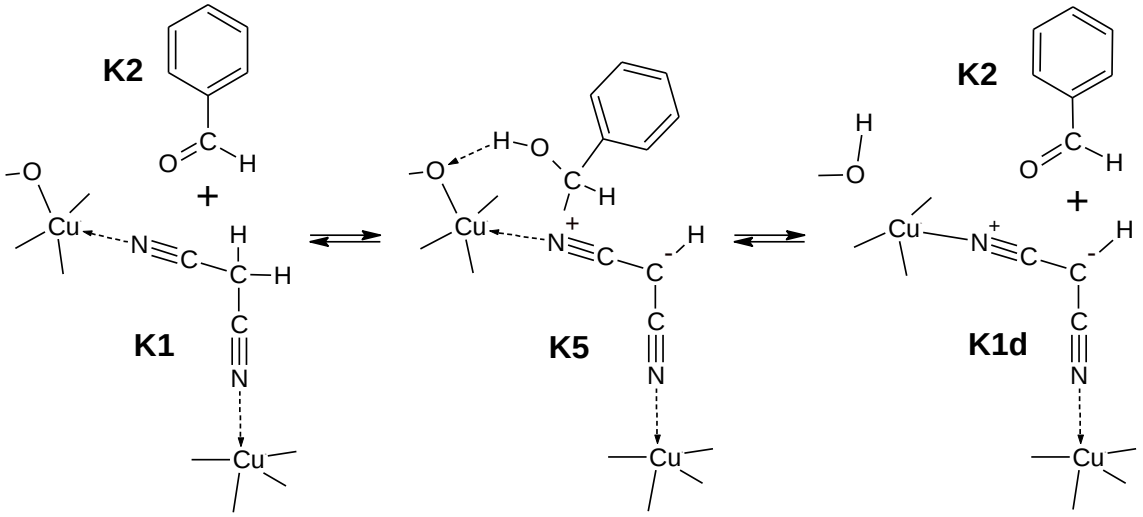

Figure 3.8 Reaction scheme of H^+ transfer from malononitrile to carboxylic group of the paddlewheel

The Knoevenagel reaction itself takes place on the carboxylic acid formed in the vicinity of immobilized **K1d** intermediate. Newly formed COOH group creates suitable interaction site for benzaldehyde with interaction energy of 93 kJ mol^{-1}. Comparing with the interaction energy of benzaldehyde with the *cus* site (25 kJ mol^{-1}) it means that interaction of benzaldehyde with Brønsted site almost entirely compensates for the energy loss due to the formation of deprotonated malononitrile and Brønsted acid site. The Knoevenagel reaction itself then proceeds along a general reaction path shown in Figure 3.6 (**K1d → K3 → K4**). After the final reaction step, dehydration, the original paddlewheel structure is fully recovered. Reaction profile obtained with the **two-pdw** cluster model and B3LYP functional is shown in Figure 3.9, together with the energies of minima on the reaction path obtained with the periodic model of CuBTC and the vdW-DF2 functional.

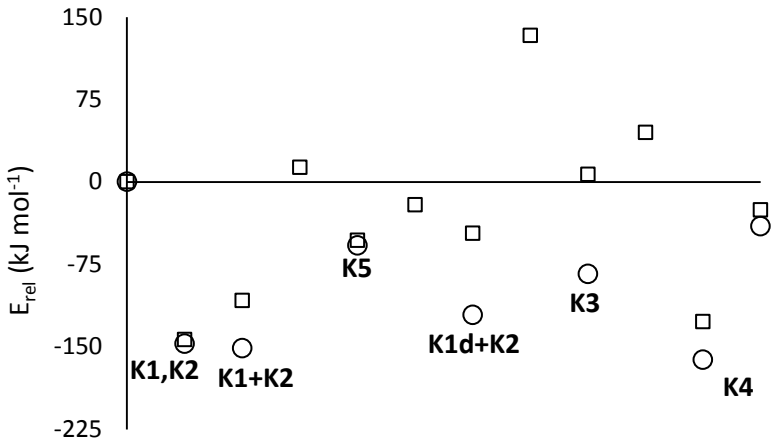

Figure 3.9 Energy profile of Knoevenagel reaction path catalyzed by CuBTC, results obtained with the **two-pdw** cluster model and B3LYP functional (□) and with the periodic model and vdW-DF2 functional (○) are reported. The x-axis is a reaction coordinate starting with non-interacting reactants and ending with non-interacting products; for notation see Figure 3.6 and Figure 3.8 captions.

The energy highest point on the reaction path is the transition state of C–C bond formation step (**K1d+K2 → K3)**, that is about 130 kJ mol^{-1} above the non-interacting reactants. The activation barrier for proton transfer and defect formation is relatively small (only 13 kJ mol^{-1} above the energy of non-interacting reactants). The calculations with periodic model of CuBTC accounting for dispersion interaction between reaction intermediates and the CuBTC catalyst show that barriers are even lower; dispersion energy provides additional stabilization. The stabilization applies mainly to the intermediates of the Knoevenagel reaction itself, providing decrease of 75 and 90 kJ mol^{-1} in relative energies of **K1d+K2** and **K3** structures respectively.

3.2.3 Discussion

The goal of this study was to explain unexpected catalytic activity of CuBTC in the Knoevenagel reaction. While CuBTC is lacking any Brønsted base needed for catalysis, it exhibits a high catalytic activity. In addition, neither reactants (malononitrile and benzaldehyde), nor mesitylene used as solvent exhibit basicity sufficient for the catalysis. It was therefore proposed that the proton has to be accepted by the CuBTC catalyst.

The dynamic formation of the defect on the paddlewheel (Figure 3.7) appears to be a key for understanding of the reaction mechanism. The adsorption of malononitrile on the *cus* sites makes the formation of defect energetically less demanding. In addition, thus formed carboxylic acid represents a strong adsorption site for benzaldehyde and the

adsorption of benzaldehyde on this Brønsted acid site almost fully compensates for the energy loss due to defect formation. The concerted effect of the reactant–catalyst interaction should be also mentioned. Deprotonation of malononitrile is mediated by benzaldehyde which, in the end of the deprotonation reaction steps stays bound to the newly formed Brønsted site. In addition, benzaldehyde adsorbed on the Brønsted site is located just next to the adsorbed deprotonated malononitrile in geometry suitable for the rate determining C–C bond formation step. Upon the dehydration reaction step the defect is healed and the product is bound only to *cus* sites.

Rather peculiar reaction mechanism described above corresponds with the experimentally found nearly 100% conversion for this reaction [85]. The reverse reaction requires formation of the defect by dissociation of water molecule into H^+ (bound to carboxylic group) and OH^- (interacting with the reaction product **K4**). Such process is much less likely than formation of the defect by malononitrile deprotonation due to both barrier heights and sterical effects.

The C–C formation step is the rate determining step on the reaction path. The structure of corresponding TS is depicted in Figure 3.10a; the partially formed **K3** intermediate is simultaneously interacting with the *cus* site and with the defect formed. The second CN group of malononitrile is no longer in interaction with the second *cus* site due to steric reasons. It should be noted that the defect plays major role in the catalysis of the individual steps in Knoevenagel reaction, as in both TS's (Figure 3.10a and b) the H^+ from this OH group is shifted towards benzaldehyde oxygen and influences the electronic structure of whole molecule.

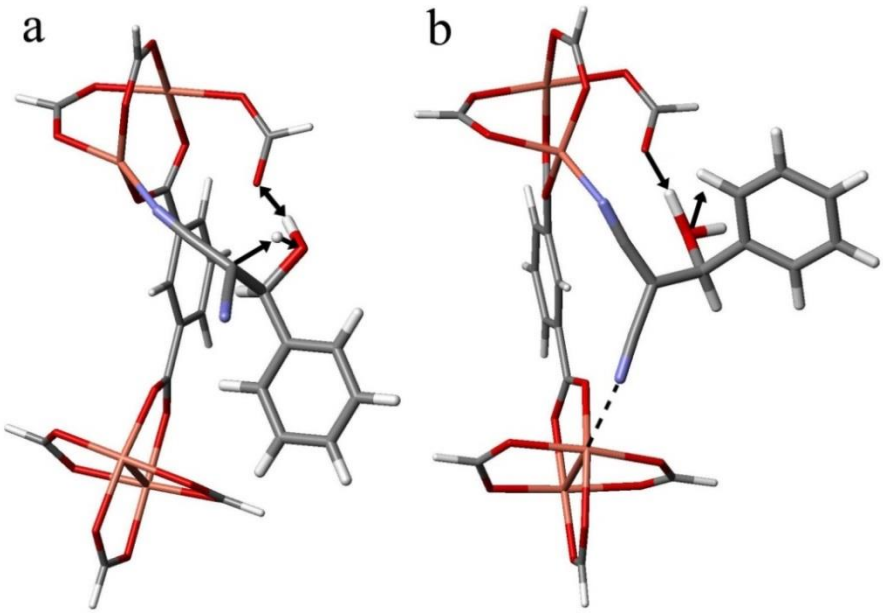

Figure 3.10 Transition states on the Knoevenagel reaction path with **two-pdw** model; a – C–C bond formation **K1d+K2 → K3**, b – dehydration **K3 → K4**

The importance of defects in reactions catalyzed by MOF has been already proposed by Vermoortele et al. for the cyclization of citronellal on Fe containing MIL-100 MOF [101]. They have first pre-treated MOF by the acid (CF_3COOH or $HClO_4$) to form Brønsted defects in the structure. Then it was tested as catalyst for the cyclization of citronellal to isopulegol. The experimental results show that the selectivity of isopulegol as product rises with the concentration of the created Brønsted sites, while overall activity of MOF is still the same and thus depending only on Lewis acidity of MIL-100. Authors proposed a "dual mechanism" in which the citronellal is adsorbed to Lewis site next to Brønsted defect and the defect is responsible for its conversion to isopulegol.

The defect formation is likely behind the catalytic activity of many MOF's that do not possess *cus* sites, for example Zn containing MOF-5 [30]. MOF-5 has been reported as a catalyst for alkylation of large polyaromatic compounds; this reaction has been found to take place inside the pores and thus depends on the presence of defect [102]. Currently accepted interpretation for this phenomenon is that the Zn–OH defects are formed by reaction with moisture. An N-methylation of aromatic amines catalyzed by $[Al_2(BDC)_3]$ is another example of a defect-catalyzed reaction [103]. All the mechanisms involving defects in catalysis by MOF's assume the existence of defects in the catalysts. However, the mechanism proposed herein for Knoevenagel reaction points out the possibility of dynamic formation of defects during the course of the reaction. As far as we know it is the first report of this type of catalytic activity of MOF's.

3.3 Intramolecular cyclization of unsaturated alcohols

The theoretical investigation of the mechanism of *cis*-dec-5-en-1-ol cyclization to heterocycles catalyzed by acidic zeolite is reported in this section. Oxygen-containing heterocyclic compounds are important components of many natural products. They are also widely used in perfumery, as flavours [104] or as insecticides [105]. Interesting examples of furans, which can be prepared by herein studied reaction, e.g., Mucoxin, compound with potential antitumor activity for breast carcinoma [106].

Oxygen containing heterocycles can be potentially very easily synthetized by the cyclization of unsaturated alcohols or dehydration of diols; however, these reactions often require use of Brønsted acids or excess of reactants [107]. Ionic liquid have been also shown to catalyse cyclization of alcohols [108]. However, only few heterogeneous catalysts have been reported as catalysts, e.g. metal(IV) phosphates [109] or material Amberlyst-15 [110].

Catalytic activity of H-BEA, H-MFI and H-FAU zeolites in cyclization of dec-5-en-1-ol was investigated experimentally by Pérez-Mayoral et al [111]. All these zeolites were shown to be efficient catalysts, providing even quantitative conversion at higher temperatures (358 K). As expected the main product of the reaction was tetrahydrofuran derivative 2-hexyltetrahydrofuran, a Markovnikov product of this reaction. The H-ZSM-5 zeolite was shown to be the best catalyst among those investigated, having the same initial conversion as other ones but showing the highest initial reaction rate (full conversion in only about 20 minutes at 358 K).

Testing of zeolites with different Si/Al ratios revealed that the reaction speed is highly dependent on aluminium content in zeolites, but the relation between S/Al and activity was rather surprising (Figure 3.11). Four different H-MFI samples were investigated, having Si/Al ratios 15, 25, 75 and 140. The efficiency of MFI catalysts at 337 K increased in order MFI/15 < MFI/25 < MFI/140 < MFI/75. It indicates that the zeolite with the highest concentration of the active sites (approximately 6 per unit cell) was far less active than zeolites with significantly smaller active site concentration. It should be noted that catalytic activity of H-zeolites is due to the presence of Brønsted acid sites.

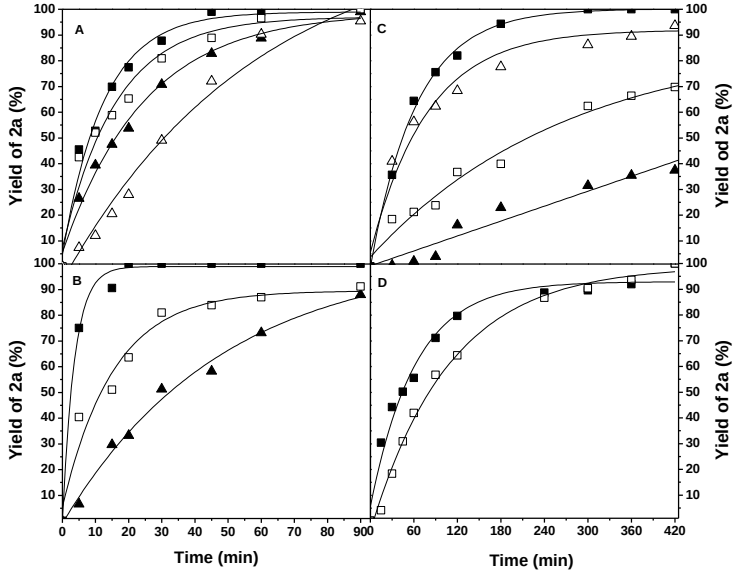

Figure 3.11 Kinetic profiles of the *cis*-4-decenol **4** cyclization reaction for zeolites with different Si/Al ratio. A) (■) BEA/37.5, (□) BEA/67.8, (▲) BEA/25 and (Δ) BEA/12.5, at 358 K. B) (■) MFI/75, (□) MFI/25 and (▲) MFI/15 at 358 K. C) (■) MFI/75, (Δ) MFI/140, (□) MFI/25 and (▲) MFI/15 at 337 K. D) (■) FAU/15 and (□) FAU/40 at 358 K. Figure from [111]

The goal of the computational study reported on herein is twofold: (i) investigation of the mechanism of catalyzed reaction and (ii) understanding of peculiar dependence of reaction rate on the Si/Al ratio. In order to lower computational demands, pen-4-en-1-ol was used as a model reactant instead of decenol. This simplification should not change the reaction mechanism and it avoids potential problems due to a large number of geometrical conformations of decenol. The results of this study together with experimental results were published in ChemSusChem [111].

3.3.1 Methods and Models

The mechanism of cyclization reaction was investigated for pent-4-en-1-ol **C1**; the reaction mechanism is shown in Figure 3.12. The H-ZSM-5 catalyst was modelled using the 3-T cluster model (Chapter 2.2). All geometries were obtained with B3LYP functional and 6-311G(d,p) basis set; more accurate MP2/cc-pVTZ calculations were performed at B3LYP/6-311G(d,p) geometries. Some stationary points were also investigated within the periodic model of H-ZSM-5 (Chapter 2.1). In the periodic model aluminium was placed into the T12 position. Calculations with periodic model were

carried out with the vdW-DF2 functional and kinetic energy cutoff of 400 eV. More details can be found in Section 2.

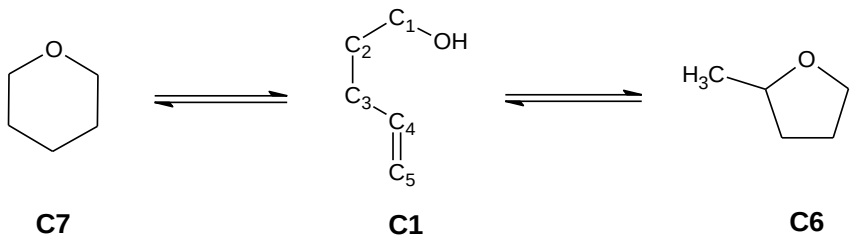

C7 **C1** **C6**

Figure 3.12 Pent-4-en-1-ol **C1** as model reactant for intramolecular cyclization reaction into 2-methyltetrahydrofuran **C6** or tetrahydropyran **C7**

3.3.2 Results

Pent-4-en-1-ol **C1** interacts with Brønsted acid sites in two different ways, thus, two different reaction precursors can be formed (Figure 3.12): the interaction between the Brønsted site and π-bond (complex **C2**) and the interaction between the Brønsted site and the OH group (complex **C3)**. Both of these adsorption complexes (reaction precursors) lead towards two main products: either Markovnikov product (2-methyltetrahydrofuran, **C6**) or anti-Markovnikov product (tetrahydropyran, C7), Figure 3.13. However, reaction takes a different course starting from precursors **C2** or **C3**.

The relative energies of minima and transition states on the reaction paths are given in Table 3.4, relative energies were calculated with respect to the non-interacting reactant **C1** and the model catalyst). Note that the interaction energy of the complex bonded by H-bond (**C3**) is nearly twice as large as that for the π-bond complex **C2**, E_{int} values are -84 kJ mol^{-1} and -45 kJ mol^{-1}, respectively.

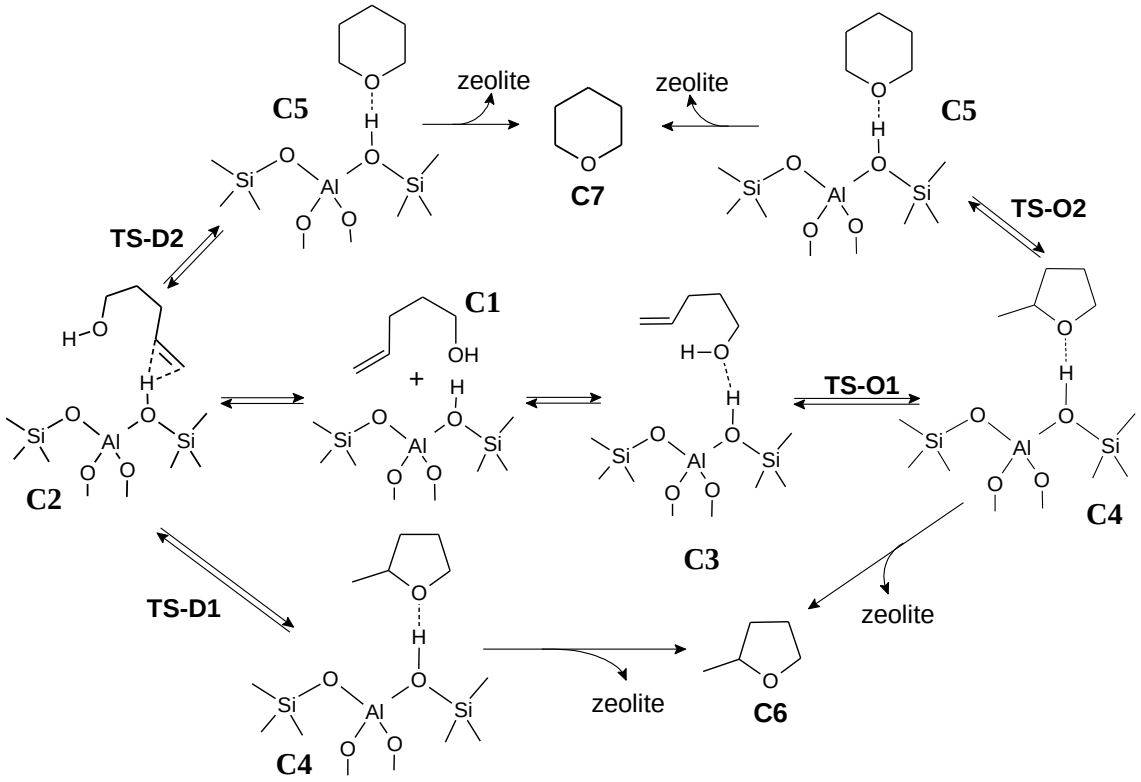

Figure 3.13 The reaction mechanisms for pent-4-en-1-ol (**C1**) conversion to 2-methyltetrahydrofuran (**C6**) and tetrahydropyran (**C7**). Reaction may proceed either via adsorption complex (reaction precursor) **C2** or **C3**. Corresponding relative energies and barrier heights are reported in Table 3.4.

The reaction paths starting from complex **C2** are described first. The π-bonded reaction precursor **C2** can be transformed directly, in a one step, either to the adsorbed methyltetrahydrofuran (**C4)** or to the adsorbed tetrahydropyran (**C5)** with activation barriers (with respect to the energy of **C2**) of 205 and 160 kJ mol^{-1}, respectively. Thus, the formation of tetrahydropyran (**C7**) is preferred over the formation of Markovnikov-rule product methyltetrahydrofuran in reaction starting from the precursor **C2**.

Table 3.4 Relative energies of the stationary points for various reaction paths.

Reaction Intermediate	Interaction via C=C		Interaction via OH	
	Structure	E_{rel} (kJ mol^{-1})[a]	Structure	E_{rel} (kJ mol^{-1})[a]
Reactant	**C2**	-45	**C3**	-84
2-methyltetrahydrofuran (**11**) formation:				
Reactant → **C6**	**TS–D1**	160	**TS–O1**	47
Adsorbed **C6**	**C4**	-154	**C4**	-154
C6 + zeolite	**C6**	-61	**C6**	-61
Tetrahydropyran (**12**) formation:				
Reactant → **C7**	**TS–D2**	115	-	-
C6 → **C7**	-	-	**TS–O2**	103
Adsorbed **C7**	**C5**	-148	**C5**	-148
C7 + zeolite	**C7**	-63	**C7**	-63

[a] Relative energies with respect to the isolated **C1** and catalyst model, energies were calculated with MP2/cc-pVTZ method using B3LYP/6-311G(d,p) geometries.

The situation is rather different for the reaction starting from the precursor **C3**. The adsorbed methyltetrahydrofuran **C4** is formed first within a single reaction step. The details of this reaction step are shown in Figure 3.14; a direct electrophilic attack of the proton from OH group on the C_5 is followed by the ring formation.

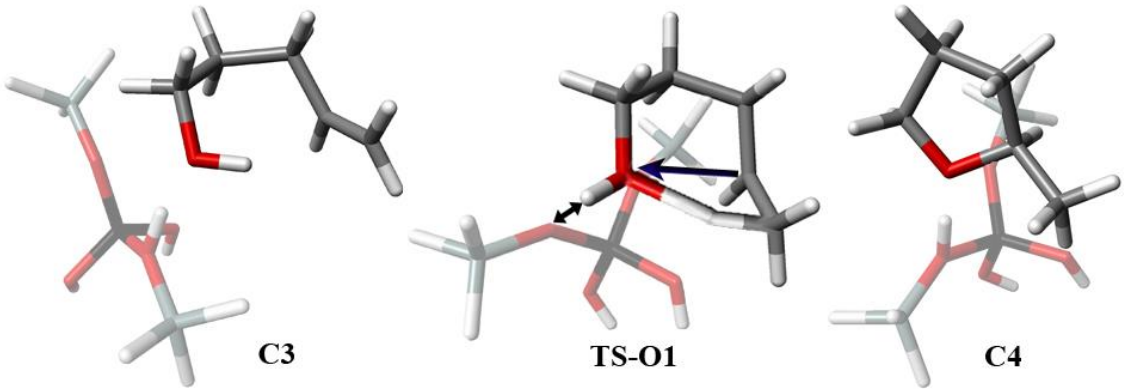

Figure 3.14 Reaction mechanism of conversion of pent-4-en-1-ol (**C1**) into 2-methyltetrahydrofuran (**C6**). The reactant interacts with the Brønsted site (complex **C3**); the activated proton of the alcohol OH group electrophilically attacks the π-orbital and, following a Markovnikov's rule, this proton transfers to C_5 while the C-O bond is being formed between C_4 and O atoms (the transition state **TS–O1**); thus formed **C6** stays adsorbed on the Brønsted site (complex **C4**).

Adsorbed methyltetrahydrofuran **C4** thus formed can subsequently desorb (as a final product) or it can undergo additional reaction step leading to the adsorbed tetrahydropyran. The direct reaction path between **C3,** and **C5** was not found; most likely due to the geometry constraints in the H transfer. The hydrogen atom from the hydroxyl group needs to be transferred to C_5 carbon (Figure 3.12) during such elementary step, and this is sterically strained process characterized by a very large

barrier. Thus, reaction precursor **C3** can only undergo a change to the complex **C4**, a reaction step characterized by the activation barrier of 131 kJ mol^{-1}. The conversion of **C4** to **C5** proceeds via the transition state characterized by activation barrier of 257 kJ mol^{-1}. For comparison, desorption of methyltetrahydrofuran (**C4**) is only about 90 kJ mol^{-1} endothermic.

Table 3.5 Comparison of interaction energies of the reactants using different models.

Reactant	Catalyst	Method	E_{int} (kJ·mol^{-1})		ΔE_{int} (kJ·mol^{-1})
			C2	C3	
C1	cluster	MP2	-45	-84	39
C8[a]	cluster	MP2	-48	-90	42
C1	MFI	vdW-DF2	-122	-160	38

[a] Relative energies of corresponding adsorption complexes formed by hex-4-en-1-ol C8.

While calculated preferences are in agreement with experimental results, a suitability of the model used still needs to be tested. To prove the suitability of the model, two aspects of the model were tested: (i) the effect of the substituent on C_5 atom of **C1** and (ii) the effect of the catalyst model. A difference between **C1** and decenol (used in experiments) is in the alkyl chain on C_5 carbon of pent-4-en-1-ol; the results obtained for hex-4-en-1-ol **C8** are reported in Table 3.5. The methyl substituent does not change significantly interaction energies of reaction precursors; therefore, their relative energies are not affected.

The effect of the zeolite catalyst model was investigated using a periodic model of H-ZSM-5. The interaction energies for adsorption complexes **C2** and **C3** obtained at the vdW-DF2 level are also reported in Table 3.5. Due to the effect of the dispersion interaction between pent-4-en-1-ol and zeolite framework the interaction energies are lowered by 77 and 76 kJ mol^{-1} for reaction precursors **C2** and **C3**, respectively. While this is a huge effect on the interaction energies, their relative values are almost unaffected.

With respect to the diameter of H-ZSM-5 channel the size of alcohol **C1** is large enough to allow its interaction with an additional acidic site on the channel surface. The pair of sites across the channel intersection was chosen arbitrarily to model such situation. This dual site interacts with both functional groups of molecule **C1**, combining interaction via double bond and OH group (Figure 3.15). The interaction energy of the resulting complex is -174 kJ mol^{-1} (compare with the results from Table 3.5).

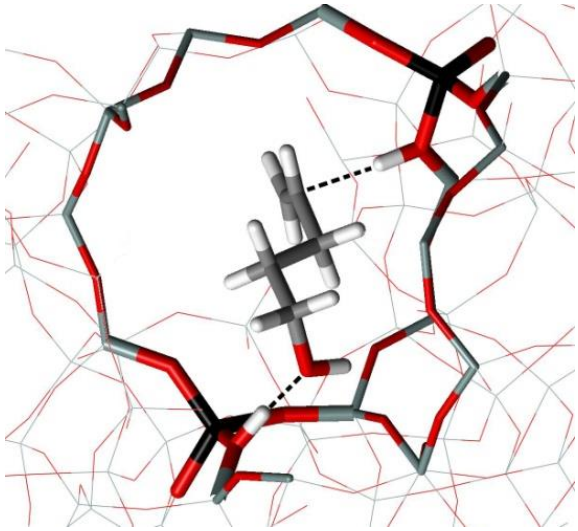

Figure 3.15 Simultaneous interaction of pent-4-en-1-ol with a pair of Brønsted sites in ZSM-5. The OH group and the π-bond interact with protons in the vicinity of framework Al in T12 and T1 positions, respectively. See caption of Fig. 8 for colouring scheme. Geometry optimized at the vdW-DF2 level.

3.3.3 Discussion

According to experimental results, reactant pent-4-en-1-ol **C1** can be transformed either into 2-methyltetrahydrofuran **C6** or into tetrahydropyran **C7**, with high selectivity toward **C6**. The selectivity is ruled by two main factors: (i) interaction energies of reaction precursors **C2** and **C3** and (ii) relative energies of activation barriers along the reaction path. Herein reported calculation show that formation of complex **C3** is energetically preferred (by about 40 kJ mol^{-1}) over the formation of complex **C2**; thus, majority of adsorbed reactant forms **C3** and the reaction paths starting from **C3** are significantly more likely than those starting from **C2**. In addition, the reaction starting from **C3** has activation barrier significantly lower than those found for reaction paths starting from **C2** (131 *vs.* 170 and 205 kJ mol^{-1}, respectively; Table 3.4). This indicates strong selectivity towards **C6** product, as only possible product of reaction from **C2**.

The interaction energies are critical in this reaction because the course of reaction is set by the relative stabilities of reaction precursors **C2** and **C3**. Interaction energies reported in Table 3.4 were obtained based on cluster-model calculations; it is therefore important to verify the reliability of the model. For that reason the reaction precursors were modelled using periodic model of H-ZSM5. The obtained results (Table 3.5) give almost the same difference between relative energies. The cluster model is thus reliable enough (in this particular case) for relative energies.

The results reported above clearly explain the reaction selectivity observed experimentally. Dependence of reaction rates on Si/Al ratio (Figure 3.11) is discussed below. A plausible explanation is based on recent observation of simultaneous

interaction of molecules with two active sites in zeolites. It has been shown that even molecules as small as CO and CO_2 may simultaneously interact with two active sites in zeolites once the concentration of active sites reaches a certain threshold [83,84]. In the case of CO adsorption in MFI such simultaneous adsorption of CO on "*dual* cation sites" was observed already for samples with Si/Al = 14 [61]. This threshold obviously has to depend on the size of the adsorbate and for alcohol **C1** having two functional groups (-OH and π-bond, both eligible for interaction with active sites) far apart, a simultaneous interaction of **C1** with two active sites can be expected for samples with Si/Al ratio even higher than 14. Therefore, the possible participation of two active sites on the interaction of zeolite with reactant was studied.

The interaction with a "dual site" was modelled by an introduction of the second aluminium into the T1 position, across the channel intersection from the original T12 Brønsted site. The interaction complex formed on such dual site is shown in Figure 3.15; the molecule stretches between the two active sites across the channel with adsorption energy of -174 kJ mol^{-1}. This interaction is 14 kJ mol^{-1} stronger than in **C3** complex and thus it is energetically preferred when such secondary active site is available. Note also that Al in T12 and T1 are just randomly selected pair of Brønsted sites and that different pairs of Brønsted sites (or a pair of Brønsted and Lewis sites) will be characterized by different interaction energy than -174 kJ mol^{-1} reported above (it can be larger or smaller).

Increase in interaction energy of reactant with the zeolite due to the presence of such secondary adsorption site will definitely affect reaction mechanism, explaining experimental decrease in catalytic activity for high-aluminium zeolites. There are at least three effects due to the presence of dual sites influencing the catalytic activity: (i) the molecule interacting with a dual site is bound more strongly (by 14 kJ mol^{-1} in situation depicted in Figure 3.15) and consequently the reaction barrier becomes higher, (ii) each functional group (OH and π-bond) of the molecule interacts with a different Brønsted site, thus, molecule is stretched between two active sites and such conformation is not favoured for the reaction due to sterical reasons (Figure 3.15), and (iii) molecules interacting with dual site will effectively block two active sites (they are not likely to undergo the reaction) and consequently they will limit the diffusion of other molecules through the zeolite channel system. Similar behaviour has been previously reported for other catalytic reactions (e.g. acylations) over zeolites and it has been proposed that the increased concentration of active sites may result in an increase in the diffusion limitations [112]. However, the interpretation of such phenomena based on simultaneous interaction of reactants/products with multiple active sites has been put forward herein for the first time.

4. Conclusions

The investigation of three different reactions catalyzed by microporous materials are reported in this study; Friedländer and Knoevenagel reactions catalyzed by CuBTC MOF and the intramolecular cyclization of unsaturated alcohols catalyzed by the H-ZSM-5 zeolite in particular. All three reactions were shown to be efficiently catalyzed by the catalyst in agreement with previous experimental results. Moreover, all these reactions show rather interesting catalytic mechanisms that take into consideration the simultaneous interaction of reactants or intermediates with more than one active site.

The Friedländer reaction of acetaldehyde and *o*-aminobenzaldehyde was previously studied in my bachelor thesis [81]. The results of previous study left some questions in the explanation of the principle of the catalytic effect of the CuBTC because the reaction was shown to be catalyzed only partially when using simple model of a single *cus* site. The follow-up study reported herein shows that the catalytic effect of CuBTC is due to the high concentration of active sites in the MOF framework, which allows the concerted effect of multiple active sites. The concerted effect was found mainly for one of the dehydration elementary steps of Friedländer reaction, during which the intermediate is adsorbed to one active site while the leaving water thus formed is directly adsorbed on the adjacent *cus* site of the adjacent *cus* site (Figure 4.1a).

The effect of two active sites was also found to be important in the Knoevenagel reaction of malononitrile and benzaldehyde. The malononitrile was found to match the distance for adsorption on the two active sites in CuBTC precisely (having the same Cu–N distance of 2.5 Å on both sides). The previously confirmed experimental activity of the CuBTC in the Knoevenagel reaction was very surprising because the malononitrile has to be deprotonated in the first step of reaction and CuBTC does not contain any basic groups. The mechanism proposed in this work suggests the formation of a dynamic defect in the structure of the CuBTC (Figure 4.1b). This defect is formed by the transfer of H^+ from malononitrile on one of the carboxylate groups, auto-catalytically mediated by the benzaldehyde. A carboxyl group is thus created within the framework and it can then catalyse the second part of the Knoevenagel reaction. The structure of CuBTC is healed in the end of the reaction as the hydrogen is consumed in the last reaction step. This interpretation corresponds very well to the experimental results showing that the CuBTC is not destroyed during the reaction. The dynamical defect formation is a very interesting phenomenon that can possibly explain activity of MOF's without free metal sites reported previously for some reactions.

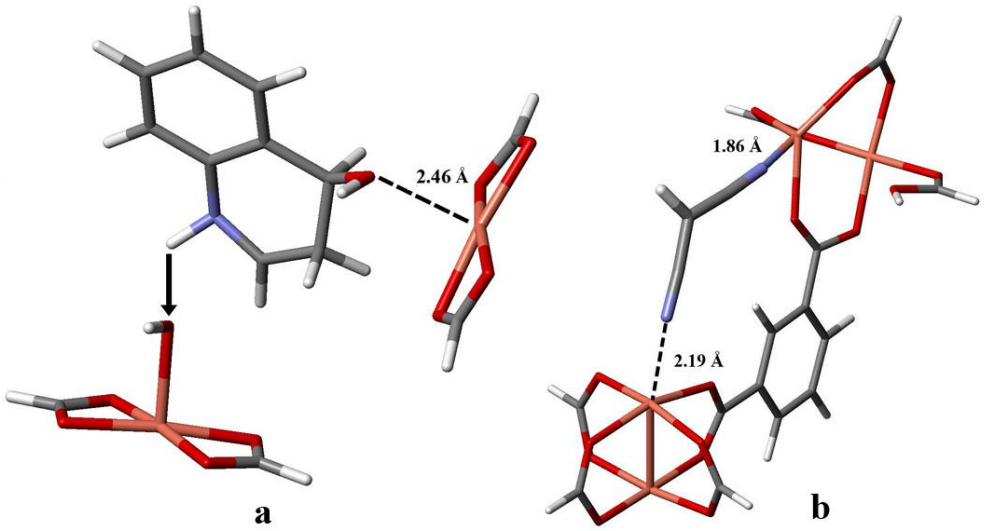

Figure 4.1 a – Structure of the first dehydration reaction step **F4a→F5** from the Friedländer reaction, the concerted effect of two active sites; b – structure of deprotonated malononitrile **K1d** adsorbed to the active site with formed defect. For further information see Chapters 3.1.2 and 3.2.2 respectively.

The mechanism of the cyclization of unsaturated alcohols was investigated as well, focusing on the understanding of peculiar decrease of catalytic activity observed for zeolites with increased concentration of Brønsted sites. The reaction of pent-5-en-1-ol studied herein can lead to two different products, 2-methyltetrahydrofuran and tetrahydropyran. It was found that the reaction preferentially provides 2-tetrahydrofuran (in agreement with experimental results). The structures of the reaction precursors were further investigated in the periodic model of H-ZSM-5. The results have shown that the reactants can easily adsorb to more than one Brønsted site in zeolites with high concentration of framework heteroatoms (Figure 3.15). The simultaneous adsorption then can cause the blocking of the active sites and limitations in the diffusion. Moreover the initial reaction barriers become higher in case of dually adsorbed reactants.

Novel reaction mechanisms involving multiple active sites have been put forward for all three reactions investigated herein. Our results suggest that the simultaneous adsorption and catalysis on multiple active sites could be a common phenomenon in the microporous materials with sufficiently high concentration of active sites. The distance between two *cus* sites in CuBTC is only 8.15 Å and molecules with two polar groups at least 5 Å apart will preferentially interact with both sites simultaneously. The dual site adsorption can also possibly explain part of the diffusion problems in zeolite channels, like in the reported cyclization reaction.

List of authored publications

1. Pérez-Mayoral E.; Musilová Z.; Gil B.; Marszalek B.; Položij M.; Nachtigall P. and Čejka J.: Synthesis of quinolines via Friedländer reaction catalyzed by CuBTC metal–organic-framework. *Dalton Transactions* 41:**40**, 4036–44 (2012).

2. Položij, M.; Pérez-Mayoral E.; Čejka J.; Hermann J. and Nachtigall P.: Theoretical investigation of the Friedländer reaction catalysed by CuBTC: Concerted effect of the adjacent Cu^{2+} sites. *Catalysis Today* 204, *Catalysis Today* **204**, 101–07 (2013).

3. Pérez-Mayoral E.; Matos I.; Nachtigall P.; Položij M., Fonseca I., Vitvarová-Procházková D. and Čejka J.: Intramolecular Hydroalkoxylation of Non-activated C-C Double Bonds Catalyzed by Zeolites: Experimental and Theoretical Study. *ChemSusChem*, **accepted**

4. Roth W.J.; Nachtigall P.; Morris R.E.; Wheatley P.S.; Seymour V.; Ashbrook S.E.; Chlubná P.; Grajciar L.; Položij M.; Zukal A.; Shvets O. and Čejka J.: A family of complex zeolites with controlled pore size prepared through a 'top down' method. *Nature Chemistry*, **accepted**

5. Bibliography

[1] Bhave, R.: *Inorganic membranes: synthesis, characteristics, and applications.* New York: Van Nostrand Reinhold, 1st ed.1991.

[2] Harold, M.; Lee, C.; Burggraaf, A. et al.: Catalysis with Inorganic Membranes. *MRS bulletin*, 34–39 (1994).

[3] Corma, A.: From Microporous to Mesoporous Molecular Sieve Materials and Their Use in Catalysis. *Chemical Reviews* **97**:6, 2373–419 (1997).

[4] Taguchi, A.; Schüth, F.: Ordered mesoporous materials in catalysis. *Microporous and Mesoporous Materials* **77**:1, 1–45 (2005).

[5] Hoffmann, F.; Cornelius, M.; Morell, J.; Fröba, M.: Silica-based mesoporous organic-inorganic hybrid materials. *Angewandte Chemie (International ed in English)* **45**:20, 3216–51 (2006).

[6] Čejka, J.; Van Bekkum, H.; Corma, A.; Schüth, F., Eds.: *Introduction to zeolite science and practice*. Amsterdam etc: Elsevier, 3rd ed.2007.

[7] Corma, A.: Inorganic Solid Acids and Their Use in Acid-Catalyzed Hydrocarbon Reactions. *Chemical Reviews* **95**:3, 559–614 (1995).

[8] Corma, A.: State of the art and future challenges of zeolites as catalysts. *Journal of Catalysis* **216**:1-2, 298–312 (2003).

[9] Clerici, M. G.; Ingallina, P.: Oxidation reactions with in situ generated oxidants. *Catalysis Today* **41**:4, 351–64 (1998).

[10] Cundy, C. S.; Cox, P. A.: The hydrothermal synthesis of zeolites: history and development from the earliest days to the present time. *Chemical reviews* **103**:3, 663–702 (2003).

[11] Kokotailo, G. T.; Lawton, S. L.; Olson, D. H.: Structure of synthetic zeolite ZSM-5. *Nature* **272**:5652, 437–38 (1978).

[12] Schüring, A.; Fritzsche, S.; Haberlandt, R. et al.: Modeling molecular diffusion in channel networks via displacements between the channel segments. *Physical Chemistry Chemical Physics* **6**:13, 3676–79 (2004).

[13] Rahimi, N.; Karimzadeh, R.: Catalytic cracking of hydrocarbons over modified ZSM-5 zeolites to produce light olefins: A review. *Applied Catalysis A: General* **398**:1-2, 1–17 (2011).

[14] Corma, A.; Huber, G. W.; Sauvanaud, L.; O'Connor, P.: Biomass to chemicals: Catalytic conversion of glycerol/water mixtures into acrolein, reaction network. *Journal of Catalysis* **257**:1, 163–71 (2008).

[15] Huber, G. W.; Corma, A.: Synergies between bio- and oil refineries for the production of fuels from biomass. *Angewandte Chemie (International ed in English)* **46**:38, 7184–201 (2007).

[16] French, R.; Czernik, S.: Catalytic pyrolysis of biomass for biofuels production. *Fuel Processing Technology* **91**:1, 25–32 (2010).

[17] Gruenert, W.; Hayes, N. W.; Joyner, R. W. et al.: Structure, Chemistry, and Activity of Cu-ZSM-5 Catalysts for the Selective Reduction of NO_x in the Presence of Oxygen. *The Journal of Physical Chemistry* **98**:42, 10832–46 (1994).

[18] Chen, H.-Y.; Sachtler, W. M.: Activity and durability of Fe/ZSM-5 catalysts for lean burn NOx reduction in the presence of water vapor. *Catalysis Today* **42**:1-2, 73–83 (1998).

[19] Férey, G.: Hybrid porous solids: past, present, future. *Chemical Society Reviews* **37**:1, 191–214 (2008).

[20] Klein, N.; Senkovska, I.; Gedrich, K. et al.: A mesoporous metal-organic framework. *Angewandte Chemie (International ed in English)* **48**:52, 9954–57 (2009).

[21] Li, H.; Eddaoudi, M.; O'Keeffe, M.; Yaghi, O. M.: Design and synthesis of an exceptionally stable and highly porous metal-organic framework **402**:6759, 276–79 (1999).

[22] Park, K. S.; Ni, Z.; Côté, A. P. et al.: Exceptional chemical and thermal stability of zeolitic imidazolate frameworks. *Proceedings of the National Academy of Sciences of the United States of America* **103**:27, 10186–91 (2006).

[23] Chui, S. S.: A Chemically Functionalizable Nanoporous Material [Cu3(TMA)2(H2O)3]n. *Science* **283**:5405, 1148–50 (1999).

[24] Li, J.-R.; Kuppler, R. J.; Zhou, H.-C.: Selective gas adsorption and separation in metal-organic frameworks. *Chemical Society Reviews* **38**:5, 1477–504 (2009).

[25] Corma, A.; García, H.; Llabrés i Xamena, F.: Engineering metal organic frameworks for heterogeneous catalysis. *Chemical reviews* **110**:8, 4606–55 (2010).

[26] Valvekens, P.; Vermoortele, F.; De Vos, D.: Metal–organic frameworks as catalysts: the role of metal active sites. *Catalysis Science & Technology* **3**:6, 1435–45 (2013).

[27] Gascon, J.; Aktay, U.; Hernandez-Alonso, M. D. et al.: Amino-based metal-organic frameworks as stable, highly active basic catalysts. *Journal of Catalysis* **261**:1, 75–87 (2009).

[28] Micek-Ilnicka, A.; Gil, B.: Heteropolyacid encapsulation into the MOF: influence of acid particles distribution on ethanol conversion in hybrid nanomaterials. *Dalton Transactions* **41**:40, 12624–29 (2012).

[29] Vermoortele, F.; Vandichel, M.; Van de Voorde, B. et al.: Electronic effects of linker substitution on Lewis acid catalysis with metal-organic frameworks. *Angewandte Chemie (International ed in English)* **51**:20, 4887–90 (2012).

[30] Ravon, U.; Domine, M. E.; Gaudillère, C. et al.: MOFs as acid catalysts with shape selectivity properties. *New Journal of Chemistry* **32**:6, 937–40 (2008).

[31] Vermoortele, F.; Ameloot, R.; Vimont, A. et al.: An amino-modified Zr-terephthalate metal-organic framework as an acid-base catalyst for cross-aldol condensation. *Chemical communications* **47**:5, 1521–23 (2011).

[32] Cirujano, F. G.; Leyva-Pérez, A.; Corma, A.; Llabrés i Xamena, F. X.: MOFs as Multifunctional Catalysts: Synthesis of Secondary Arylamines, Quinolines, Pyrroles, and Arylpyrrolidines over Bifunctional MIL-101. *ChemCatChem* **5**:2, 538–49 (2013).

[33] Arnanz, A.; Pintado-Sierra, M.; Corma, A. et al.: Bifunctional Metal Organic Framework Catalysts for Multistep Reactions: MOF-Cu(BTC)-[Pd] Catalyst for One-Pot Heteroannulation of Acetylenic Compounds. *Advanced Synthesis & Catalysis* **354**:7, 1347–55 (2012).

[34] Pan, Y.; Yuan, B.; Li, Y.; He, D.: Multifunctional catalysis by Pd@MIL-101: one-step synthesis of methyl isobutyl ketone over palladium nanoparticles deposited on a metal-organic framework. *Chemical communications (Cambridge, England)* **46**:13, 2280–82 (2010).

[35] Srirambalaji, R.; Hong, S.; Natarajan, R. et al.: Tandem catalysis with a bifunctional site-isolated Lewis acid-Brønsted base metal-organic framework, NH2-MIL-101(Al). *Chemical Communications* **48**:95, 11650–52 (2012).

[36] Wu, P.; Wang, J.; Li, Y. et al.: Luminescent Sensing and Catalytic Performances of a Multifunctional Lanthanide-Organic Framework Comprising a Triphenylamine Moiety. *Advanced Functional Materials* **21**:14, 2788–94 (2011).

[37] Chowdhury, P.; Bikkina, C.; Meister, D. et al.: Comparison of adsorption isotherms on Cu-BTC metal organic frameworks synthesized from different routes. *Microporous and Mesoporous Materials* **117**:1-2, 406–413 (2009).

[38] Schlichte, K.; Kratzke, T.; Kaskel, S.: Improved synthesis, thermal stability and catalytic properties of the metal-organic framework compound $Cu_3(BTC)_2$. *Microporous and Mesoporous Materials* **73**:1-2, 81–88 (2004).

[39] Alaerts, L.; Séguin, E.; Poelman, H. et al.: Probing the Lewis acidity and catalytic activity of the metal-organic framework $[Cu_3(btc)_2]$ (BTC=benzene-1,3,5-tricarboxylate). *Chemistry a Europian Journal* **12**:28, 7353–63 (2006).

[40] Mueller, U.; Schubert, M.; Teich, F. et al.: Metal–organic frameworks—prospective industrial applications. *Journal of Materials Chemistry* **16**:7, 626 (2006).

[41] Czaja, A. U.; Trukhan, N.; Müller, U.: Industrial applications of metal-organic frameworks. *Chemical Society Reviews* **38**:5, 1284–93 (2009).

[42] Cramer, C.: *Essentials of computational chemistry : theories and models*. West Sussex England; New York: J. Wiley, 1st ed.2002.

[43] Grimme, S.: Semiempirical GGA-type density functional constructed with a long-range dispersion correction. *Journal of Computational Chemistry* **27**:15, 1787–99 (2006).

[44] Klimeš, J.; Bowler, D. R.; Michaelides, A.: Van der Waals density functionals applied to solids. *Physical Review B* **83**:19, 195131–42 (2011).

[45] Valenzano, L.; Civalleri, B.; Chavan, S. et al.: Disclosing the Complex Structure of UiO-66 Metal Organic Framework: A Synergic Combination of Experiment and Theory. *Chemistry of Materials* **23**:7, 1700–18 (2011).

[46] Bludský, O.; Silhan, M.; Nachtigall, P. et al.: Theoretical investigation of CO interaction with copper sites in zeolites: periodic DFT and hybrid quantum mechanical/interatomic potential function study. *The journal of physical chemistry B* **109**:19, 9631–38 (2005).

[47] Nachtigall, P.; Delgado, M. R.; Nachtigallova, D.; Arean, C. O.: The nature of cationic adsorption sites in alkaline zeolites-single, dual and multiple cation sites. *Physical chemistry chemical physics : PCCP* **14**:5, 1552–69 (2012).

[48] Tuma, C.; Sauer, J.: Treating dispersion effects in extended systems by hybrid MP2:DFT calculations-protonation of isobutene in zeolite ferrierite. *Physical chemistry chemical physics : PCCP* **8**:34, 3955–65 (2006).

[49] Chen, L.; Grajciar, L.; Nachtigall, P.; Düren, T.: Accurate Prediction of Methane Adsorption in a Metal–Organic Framework with Unsaturated Metal Sites by Direct Implementation of an ab Initio Derived Potential Energy Surface in GCMC Simulation. *The Journal of Physical Chemistry C* **115**:46, 23074–80 (2011).

[50] Lee, C.; Yang, W.; Parr, R. G.: Development of the Colle-Salvetti correlation-energy formula into a functional of the electron density. *Physical Review B* **37**:2, 785–89 (1988).

[51] Becke, A. D.: Density-functional thermochemistry. III. The role of exact exchange. *The Journal of Chemical Physics* **98**:7, 5648–52 (1993).

[52] Simón, L.; Goodman, J. M.: How reliable are DFT transition structures? Comparison of GGA, hybrid-meta-GGA and meta-GGA functionals. *Organic & Biomolecular chemistry* **9**:3, 689–700 (2011).

[53] Lynch, B. J.; Truhlar, D. G.: How Well Can Hybrid Density Functional Methods Predict Transition State Geometries and Barrier Heights? *The Journal of Physical Chemistry A* **105**:13, 2936–41 (2001).

[54] Blaszkowski, S. R.; Van Santen, R. A.: The Mechanism of Dimethyl Ether Formation from Methanol Catalyzed by Zeolitic Protons. *Journal of the American Chemical Society* **118**:21, 5152–53 (1996).

[55] Boronat, M.; Viruela, P. M.; Corma, A.: Reaction intermediates in acid catalysis by zeolites: prediction of the relative tendency to form alkoxides or carbocations as a function of hydrocarbon nature and active site structure. *Journal of the American Chemical Society* **126**:10, 3300–09 (2004).

[56] Boronat, M.; Corma, A.; Renz, M.: Mechanism of the Meerwein-Ponndorf-Verley-Oppenauer (MPVO) redox equilibrium on Sn- and Zr-beta zeolite catalysts. *The journal of physical chemistry B* **110**:42, 21168–74 (2006).

[57] Hansen, N.; Kerber, T.; Sauer, J. et al.: Quantum chemical modeling of benzene ethylation over H-ZSM-5 approaching chemical accuracy: a hybrid MP2:DFT study. *Journal of the American Chemical Society* **132**:33, 11525–38 (2010).

[58] Cortese, R.; Duca, D.: A DFT study of IRMOF-3 catalysed Knoevenagel condensation. *Physical chemistry chemical physics* **13**:35, 15995–16004 (2011).

[59] Chizallet, C.; Lazare, S.; Bazer-Bachi, D. et al.: Catalysis of transesterification by a nonfunctionalized metal-organic framework: acido-basicity at the external surface of ZIF-8 probed by FTIR and ab initio calculations. *Journal of the American Chemical Society* **132**:35, 12365–77 (2010).

[60] Grajciar, L.; Bludský, O.; Nachtigall, P.: Water Adsorption on Coordinatively Unsaturated Sites in CuBTC MOF. *The Journal of Physical Chemistry Letters* **1**:23, 3354–59 (2010).

[61] Arean, C. O.; Delgado, M. R.; Frolich, K. et al.: Computational and Fourier Transform Infrared Spectroscopic Studies on Carbon Monoxide Adsorption on the Zeolites Na-ZSM-5 and K-ZSM-5: Evidence of Dual-Cation Sites. *Journal of Physical Chemistry C* **112**:12, 4658–66 (2008).

[62] Perdew, J. P.; Burke, K.; Ernzerhof, M.: Generalized Gradient Approximation Made Simple. *Physical Review Letters* **77**:18, 3865–68 (1996).

[63] Lee, K.; Murray, É. D.; Kong, L. et al.: Higher-accuracy van der Waals density functional. *Physical Review B* **82**:8, 81101–04 (2010).

[64] Blöchl, P. E.: Projector augmented-wave method. *Physical Review B* **50**:24, 17953–79 (1994).

[65] Kresse, G.; Joubert, D.: From ultrasoft pseudopotentials to the projector augmented-wave method. *Physical Review B* **59**:3, 1758–75 (1999).

[66] Kresse, G.; Hafner, J.: Ab initio molecular dynamics for open-shell transition metals. *Physical Review B* **48**:17, 13115–18 (1993).

[67] Frisch, G. W. T. M. J.; Schlegel, H. B.; Scuseria, G. E. et al.: *Gaussian 09*. Pittsburgh, PA: Gaussian, Inc., 2009.

[68] Krishnan, R.; Binkley, J. S.; Seeger, R.; Pople, J. A.: Self-consistent molecular orbital methods. XX. A basis set for correlated wave functions. *The Journal of Chemical Physics* **72**:1, 650–54 (1980).

[69] Dunning, T. H.: Gaussian basis sets for use in correlated molecular calculations. I. The atoms boron through neon and hydrogen. *The Journal of Chemical Physics* **90**:2, 1007–23 (1989).

[70] Marco-Contelles, J.; Pérez-Mayoral, E.; Samadi, A. et al.: Recent advances in the Friedländer reaction. *Chemical Reviews* **109**:6, 2652–71 (2009).

[71] Chauhan, P.; Srivastava, S.: Present trends and future strategy in chemotherapy of malaria. *Current medicinal chemistry* **8**:13, 1535–42 (2001).

[72] Psomas, G.; Kessissoglou, D. P.: Quinolones and non-steroidal anti-inflammatory drugs interacting with copper(II), nickel(II), cobalt(II) and zinc(II): structural features, biological evaluation and perspectives. *Dalton transactions* **42**:18, 6252–76 (2013).

[73] Dubé, D.; Blouin, M.; Brideau, C. et al.: Quinolines as potent 5-lipoxygenase inhibitors: synthesis and biological profile of L-746,530. *Bioorganic & medicinal chemistry letters* **8**:10, 1255–60 (1998).

[74] Madapa, S.; Tusi, Z.; Batra, S.: Advances in the Syntheses of Quinoline and Quinoline-Annulated Ring Systems. *Current Organic Chemistry* **12**:13, 1116–83 (2008).

[75] Cheng, C.-C.; Yan, S.-J.: *The Friedländer Synthesis of Quinolines*. John Wiley & Sons, Inc., 2004.

[76] De, S. K.; Gibbs, R. A.: A mild and efficient one-step synthesis of quinolines. *Tetrahedron Letters* **46**:10, 1647–49 (2005).

[77] Arumugam, P.; Karthikeyan, G.; Atchudan, R. et al.: A Simple, Efficient and Solvent-Free Protocol for the Friedländer Synthesis of Quinolines by Using SnCl22H2O. *Chemistry Letters* **34**:3, 314–15 (2005).

[78] López-Sanz, J.; Pérez-Mayoral, E.; Procházková, D. et al.: Zeolites Promoting Quinoline Synthesis via Friedländer Reaction. *Topics in Catalysis* **53**:19-20, 1430–37 (2010).

[79] Pérez-Mayoral, E.; Čejka, J.: [Cu3(BTC)2]: A Metal-Organic Framework Catalyst for the Friedländer Reaction. *ChemCatChem* **3**:1, 157–59 (2011).

[80] Pérez-Mayoral, E.; Musilová, Z.; Gil, B. et al.: Synthesis of quinolines via Friedländer reaction catalyzed by CuBTC metal-organic-framework. *Dalton Transactions* **41**:14, 4036–44 (2012).

[81] Položij, M.: *Teoretické studium Friedländerovy reakce katalyzované materiálem CuBTC*. Charles university in Prague: Bachelor thesis, 2011.

[82] Položij, M.; Pérez-Mayoral, E.; Čejka, J. et al.: Theoretical investigation of the Friedländer reaction catalysed by CuBTC: Concerted effect of the adjacent Cu2+ sites. *Catalysis Today* **204**, 101–07 (2013).

[83] Zukal, A.; Pulido, A.; Gil, B. et al.: Experimental and theoretical determination of adsorption heats of CO2 over alkali metal exchanged ferrierites with different Si/Al ratio. *Physical chemistry chemical physics* **12**:24, 6413–22 (2010).

[84] Garrone, E.; Bulánek, R.; Frolich, K. et al.: Single and dual cation sites in zeolites: theoretical calculations and FTIR spectroscopic studies on CO adsorption on K-FER. *The Journal of Physical Chemistry B* **110**:45, 22542–50 (2006).

[85] Opanasenko, M.; Dhakshinamoorthy, A.; Shamzhy, M. et al.: Comparison of the catalytic activity of MOFs and zeolites in Knoevenagel condensation. *Catalysis Science & Technology* **3**:2, 500–07 (2013).

[86] Tietze, L. F.: Domino Reactions in Organic Synthesis. *Chemical Reviews* **96**:1, 115–36 (1996).

[87] Lai, S. M.; Ng, C. P.; Martin-Aranda, R.; Yeung, K. L.: Knoevenagel condensation reaction in zeolite membrane microreactor. *Microporous and Mesoporous Materials* **66**:2-3, 239–52 (2003).

[88] Corma, A.; Fornés, V.; Martín-Aranda, R. M. et al.: Zeolites as base catalysts: Condensation of aldehydes with derivatives of malonic esters. *Applied Catalysis* **59**:1, 237–48 (1990).

[89] Wirz, R.; Ferri, D.; Baiker, A.: ATR-IR spectroscopy of pendant NH_2 groups on silica involved in the Knoevenagel condensation. *Langmuir* **22**:8, 3698–706 (2006).

[90] Prajapati, D.; Lekhok, K. C.; Sandhu, J. S.; Ghosh, A. C.: Lithium bromide as a new catalyst for carbon-carbon bond formation in the solid state. *Journal of the Chemical Society, Perkin Transactions 1* **25**:9, 959–60 (1996).

[91] Corma, A.; Fornés, V.; Martín-Aranda, R. M.; Rey, F.: Determination of base properties of hydrotalcites: Condensation of benzaldehyde with ethyl acetoacetate. *Journal of Catalysis* **134**:1, 58–65 (1992).

[92] Kantam, M.; Choudary, B. M.; Reddy, C. V. et al.: Aldol and Knoevenagel condensations catalysed by modified Mg–Al hydrotalcite: a solid base as catalyst useful in synthetic organic chemistry. *Chemical Communications*:9, 1033–34 (1998).

[93] Bigi, F.; Chesini, L.; Maggi, R.; Sartori, G.: Montmorillonite KSF as an Inorganic, Water Stable, and Reusable Catalyst for the Knoevenagel Synthesis of Coumarin-3-carboxylic Acids. *The Journal of Organic Chemistry* **64**:3, 1033–35 (1999).

[94] Kantevari, S.; Bantu, R.; Nagarapu, L.: $HClO_4$–SiO_2 and PPA–SiO_2 catalyzed efficient one-pot Knoevenagel condensation, Michael addition and cyclo-dehydration of dimedone and aldehydes in acetonitrile, aqueous and solvent free conditions: Scope and limitations. *Journal of Molecular Catalysis A: Chemical* **269**:1-2, 53–57 (2007).

[95] Chen, X.; Arruebo, M.; Yeung, K. L.: Flow-synthesis of mesoporous silicas and their use in the preparation of magnetic catalysts for Knoevenagel condensation reactions. *Catalysis Today* **204**, 140–47 (2013).

[96] Dong, X.; Hui, Y.; Xie, S. et al.: Schiff base supported MCM-41 catalyzed the Knoevenagel condensation in water. *RSC Advances* **3**:10, 3222–26 (2013).

[97] Reddy, T. I.; Varma, R. S.: Rare-earth (RE) exchanged NaY zeolite promoted knoevenagel condensation. *Tetrahedron Letters* **38**:10, 1721–24 (1997).

[98] Dhakshinamoorthy, A.; Opanasenko, M.; Čejka, J.; Garcia, H.: Metal Organic Frameworks as Solid Catalysts in Condensation Reactions of Carbonyl Groups. *Advanced Synthesis & Catalysis* **355**:2-3, 247–68 (2013).

[99] Llabrés i Xamena, F. X.; Cirujano, F. G.; Corma, A.: An unexpected bifunctional acid base catalysis in IRMOF-3 for Knoevenagel condensation reactions. *Microporous and Mesoporous Materials* **157**, 112–17 (2012).

[100] Hartmann, M.; Fischer, M.: Amino-functionalized basic catalysts with MIL-101 structure. *Microporous and Mesoporous Materials* **164**, 38–43 (2012).

[101] Vermoortele, F.; Ameloot, R.; Alaerts, L. et al.: Tuning the catalytic performance of metal–organic frameworks in fine chemistry by active site engineering. *Journal of Materials Chemistry* **22**:20, 10313–21 (2012).

[102] Ravon, U.; Savonnet, M.; Aguado, S. et al.: Engineering of coordination polymers for shape selective alkylation of large aromatics and the role of defects. *Microporous and Mesoporous Materials* **129**:3, 319–29 (2010).

[103] Dhakshinamoorthy, A.; Alvaro, M.; Garcia, H.: Metal organic frameworks as heterogeneous catalysts for the selective N-methylation of aromatic primary amines with dimethyl carbonate. *Applied Catalysis A: General* **378**:1, 19–25 (2010).

[104] Narula, A. P. S.: The Search for New Fragrance Ingredients. *Perfumer & Flavorist* **28**:4, 62–73 (2003).

[105] Rodriguez-Saona, C.; Maynard, D. F.; Phillips, S.; Trumble, J. T.: Avocadofurans and Their Tetrahydrofuran Analogues: Comparison of Growth Inhibitory and Insecticidal Activity. *Journal of Agricultural and Food Chemistry* **48**:8, 3642–45 (2000).

[106] Mohapatra, D. K.; Mohapatra, S.; Gurjar, M. K.: Double intramolecular oxymercuration: stereoselective synthesis of highly substituted bis-tetrahydrofuran. *Tetrahedron Letters* **47**:33, 5943–47 (2006).

[107] Carr, G.; Whittaker, D.: Cyclic ether formation in superacid media. *Journal of the Chemical Society, Perkin Transactions 2* **28**:4, 359 (1989).

[108] Dzudza, A.; Marks, T. J.: Efficient intramolecular hydroalkoxylation/cyclization of unactivated alkenols mediated by lanthanide triflate ionic liquids. *Organic Letters* **11**:7, 1523–26 (2009).

[109] Al-Qallaf, F. A. H.; Hodson, L. F.; Johnstone, R. A. W. et al.: Heterogeneous liquid phase catalysis by metal (IV) phosphates of cyclic ether formation and a reverse Prins reaction. *Journal of Molecular Catalysis A: Chemical* **152**:1-2, 187–200 (2000).

[110] Franck, X.; Figadére, B.; Cavé, A.: From intermolecular alcohol additions on a double bond to electrocyclizations of non-activated γ, δ-unsaturated alcohols: An easy synthesis of tetrahydrofurans. *Tetrahedron Letters* **38**:8, 1413–14 (1997).

[111] Pérez-mayoral, E.; Matos, I.; Nachtigall, P. et al.: Intramolecular Hydroalkoxylation of Non-activated C-C Double Bonds Catalyzed by Zeolites : Experimental and Theoretical Study, accepted.

[112] Beers, A. E. W.; Nijhuis, T. A.; Kapteijn, F.; Moulijn, J. A.: Zeolite coated structures for the acylation of aromatics. *Microporous and Mesoporous Materials* **48**:1-3, 279–84 (2001).